X-RAY ANALYSIS OF FATIGUE DAMAGE IN COPPER

by

ROY GENE BAGGERLY

A thesis submitted in partial fulfillment

of the requirements for the degree of

MASTER OF SCIENCE

in

METALLURGICAL ENGINEERING

UNIVERSITY OF WASHINGTON

1966

Approved by _____

Department School of Mineral Engineering

Date _____

TABLE OF CONTENTS

LIST OF FIGURES

ABSTRACT

A Warren-Averbach[1-4] x-ray line profile analysis was applied to broadened x-ray diffraction peaks from copper deformed in fatigue. The copper specimens were fatigued by four point bending at various strain amplitudes, and measurements were made at various fractions of the total fatigue life. The analysis results in an estimation of 1) an average coherently diffracting domain size in a direction normal to the diffracting planes; and 2) a strain distribution function. The strain distribution function is in terms of the root mean square strain, $\langle \epsilon^2 \rangle^{1/2}$ where ϵ is averaged over a given distance at all points in the diffracting crystals. This rms strain is expressed as a function of averaging distance for a direction normal to the diffracting planes.

The rms strains were found to be a function of the fatigue strain amplitude level, increasing with amplitude and reaching a maximum limiting value during the first 2% of the fatigue life. The strains were normally larger in the <100> direction compared to the <111> direction and the absolute values were quite small. These results may be explained by assuming the dislocations are present in the form of dipoles because the lattice strain around a dipole is much less than around single dislocations.

Conclusions arrived at in this analysis are in agreement with current theories of fatigue damage in metals. The result that maximum hardening is achieved during the initial few percent of the fatigue life is confirmed by many other investigators using entirely different analytical techniques[5]. It is felt that the structure of the material is changing during this initial hardening stage to an eventual steady state characteristic of the testing conditions. A unique substructure is developed which thereafter persists, and the remainder of the fatigue test is taken up by crack propagation through this substructure until ultimate failure occurs by fracture. The formation of this steady state structure is dependent on the maximum fatigue strain amplitude and on the frequency and temperature of cycling for a particular material.

ACKNOWLEDGEMENTS

The author is greatfully indebted to Dr. William F. Flanagan whose encouragement and many valuable discussions made this thesis possible. The suggestions and discussions with Dr. Regis Pelloux from The Boeing Co. are also greatly appreciated.

The author also wishes to thank Dr. K.R. Evans and D.J. Bailey for their help in preparing the computer program and to The Boeing Co. who provided the x-ray diffraction equipment and fatigue machine for the experimental investigation.

This work was partially supported from funds made available to the University of Washington through NASA Grant 484 -- "Multidisciplinary Research on the Nature and Properties of Ceramic Materials".

INTRODUCTION

Many aspects of metal fatigue have been investigated using various analytical techniques such as transmission electron microscopy, internal friction, electrical resistivity and optical microscopy. The use of x-ray diffraction techniques in studying fatigue tends to relate bulk properties such as the fatigue limit with the local substructure observed by electron microscopy because the volume examined with x-rays is quite large and results are averaged on an atomic scale. Nearly all previous attempts of using x-ray diffraction for this application have been concerned with interpreting back reflection x-ray diffraction photographs. Exceptions to this have been the work by S. Moll[6] and R.J. Hartmann and E. Macherauch[7]; both applied the Warren-Averbach analysis[1-4] to the study of fatigue damage in nickel. Since nickel has a relatively large stacking fault energy ($\gamma \sim 150$ ergs/cm^2)[8] a similar study conducted on a metal having a lower stacking fault energy, viz. copper ($\gamma \sim 40$ ergs/cm^2)[8], would be of value in elucidating the mechanism of metal fatigue. This is due to the fact that stacking fault energies have a marked effect[5,9,10] on fatigue characteristics such as dislocation structure and endurance limit, i.e. the limit increases with decreasing stacking fault energy, and fatigue hardening is markedly similar to three-stage tensile hardening expected for FCC single crystals.

Transmission electron microscopy has shown[11-15] that for low strain amplitude fatigue, i.e. failure in approximately 10^5 or more cycles, numerous dislocation dipoles are formed. These are parallel and clustered in dense regions parallel to $\{111\}$ planes. Separating these dense clusters is a region of low dislocation density. The Burgers vectors of dislocation dipoles in a cluster as shown by electron diffraction are aligned and the dipoles are elongated in a $\langle 112 \rangle$ direction when the crystal is oriented for single slip; if the crystal is oriented for multiple slip more nearly equiaxed loops are observed. A lack of well defined cell structure is typical of this low strain amplitude range, which may be contrasted to high strain amplitude fatigue where the substructure is more nearly comparable to the substructure which forms during unidirectional loading. For the latter case, i.e. strain amplitude levels where failure occurs in approximately 10^3 cycles

or less, a definite cell structure develops and a general increase in dislocation tangles is present. Since the strain field around a dislocation dipole decreases as the inverse square of the distance, compared to that of a single dislocation whose strain field decreases as the inverse of the distance, a structure containing dipoles would not be expected to broaden the x-ray diffraction profiles as drastically as an equal density of dislocations present in the form of tangles. Also, since dipoles are elongated in a <112> direction, the strain distribution and coherently diffracting domain size would be expected to be anisotropic in the fatigued crystal. Thus, it might be expected that the results of the x-ray diffraction analysis would be influenced by a change in fatigue strain amplitude.

This thesis concerns itself with a determination of the substructure developed during fatigue cycling for the ultimate purpose of providing us with a better understanding of its effect on crack propagation and failure. Substructure is here defined by an average coherently diffracting domain size and an rms strain distribution as determined by the Warren-Averbach analysis[1-4]. This substructure (or these parameters) are examined as a function of the percent fatigue life and strain amplitude of the fatigue specimens.

X-RAY ANALYSIS

X-ray diffraction peaks in the Warren-Averbach analysis[1-4] are represented by a Fourier series, and a Stokes analysis[16] is performed on the Fourier coefficients of the cold-worked and annealed peaks resulting in the Fourier coefficients of a broadening function. This function is free from all forms of instrumental broadening inherent in the experimental technique, including for example the $K\alpha_1$ - $K\alpha_2$ doublet broadening which makes further correction for the doublet unnecessary.

The intensity of an x-ray diffraction peak expressed as a Fourier series is given by:

$$I = K(\theta)\, N \sum_{-\infty}^{\infty} \{A_n \cos(2\pi n h_3) + B_n \sin(2\pi n h_3)\} \qquad (1)$$

θ = Bragg angle

$N = N_1 N_2 N_3$ = number of unit cells in the diffracting crystal

N_3 = average number of unit cells in a coherent diffracting column normal to the diffracting planes

h_3 = continuous variable designating a position in the unit cell

A_n and B_n are coefficients which for the broadening function alone can be rewritten as:

$$A_n = \frac{N_n}{N_3} \langle \cos(2\pi l Z_n) \rangle \qquad (2)$$

$$B_n = \frac{-N_n}{N_3} \langle \sin(2\pi l Z_n) \rangle \qquad (3)$$

where:

l = (00l) reflection*

Z_n = the displacement of n unit cells from the strain free position.

---

* For any (hkl) plane from a cubic crystal it is possible to adopt orthorhombic axes to change the form of the plane to (00l). This is done to simplify the mathematics.

Stacking faults lead to an asymmetry in the broadening function[4], but in the absence of stacking faults the broadening is symmetrical about the origin allowing us to neglect the imaginary or sin coefficients of the Fourier series (they will approximate zero). Also, the symmetry of our broadened peaks and evidence in the literature allow us to disregard fault broadening.

Considering the cos coefficient in more detail we see from equation (2) that it can be represented as the product of two coefficients, one relating to coherent domain size and one to rms strain. Thus,

$$A_n = A_n^S A_n^D \qquad (4)$$

where

$$A_n^S = \frac{N_n}{N_3} = \text{domain size coefficient} \qquad (5)$$

$$A_n^D = \langle \cos(2\pi l Z_n) \rangle \cong (1 - 2\pi^2 l^2 \langle Z_n^2 \rangle) = \text{distortion coefficient assuming relatively small values of } Z_n \qquad (6)$$

Since $N_n = N_3$ and $Z_n = 0$ for $n = 0$, both coefficients are normalized to unity for $n = 0$, hence A_n is also normalized to unity for $n = 0$.

N_n can be defined as:

$$N_n = \int_{i=n}^{\infty} (i-n)\, \rho_i \, di \qquad (7)$$

where ρ_i is the fraction of columns of length i cells. Differentiating A_n^S with respect to n results in:

$$\frac{d A_n^S}{dn} = \frac{-1}{N_3} \int_{i=n}^{\infty} \rho_i \, di = \frac{-1}{N_3} \Big]_{n=0} \qquad (8)$$

which shows that the negative initial slope of a plot of A_n^S vs. n gives directly the average coherent domain size N_3.[4]

The distortion coefficient can be rewritten explicitly in terms of the planar indices (hkl). If we let $l_o^2 = h^2 + k^2 + l^2$, $\Delta L = a_3 Z_n$, and $a_3/l = d = a_o/l_o$ where a_o is the lattice parameter, the distortion coefficient becomes:

$$A_L^D = (1 - 2\pi^2 l_o^2 \langle \Delta L^2 \rangle / a_o^2) \qquad (9)$$

The domain size coefficients and distortion coefficients can be separated by expressing A_n in logarithmic form.

$$\ln A_L = \ln A_L^S - 2\pi^2 l_o^2 \langle \Delta L^2 \rangle / a_o^2 \qquad (10)$$

Thus when $\ln A_L$ is plotted vs. l_o^2 for specific values of L, the resulting slopes and intercepts can be evaluated to arrive at an average coherently diffracting domain size in the crystal and an rms strain distribution function.

EXPERIMENTAL PROCEDURE

Material

The copper used in this investigation was OFHC copper sheet produced by Anaconda American Brass Co. having dimensions of 12" x 23" x 0.0622" and a grain size of approximately 0.0003". It was reported to have been lightly cold rolled to approximately 6% reduction in thickness. This sheet was subsequently sheared into 6" x 3½" blanks; the blanks were then pickled in 20% HNO_3, cross-rolled to a thickness of 0.045" and then rolled in one direction to 0.040" by 0.005" steps. This produced a good surface finish and a total thickness reduction of 40%. Fatigue specimens were then machined (c.f. Figure 1) from the cold rolled blanks, pickled in 20% HNO_3, and annealed in a salt bath for 5 minutes at 750°F. This anneal resulted in a recrystallized equiaxed grain size of 0.0004" and an oxidized surface on the specimens which was easily removed by electropolishing in 60% Phosphoric acid - 40% N-Butyl alcohol at a temperature of 190°F with a 7 - 8 volts potential. A mirror surface was achieved on electropolishing which was more than adequate for x-ray diffraction analysis.

The degree of preferred orientation present in the fatigue specimens was determined by preparing {111} and {200} pole figures for the copper in both the cold-rolled and recrystallized condition (c.f. Figure 2). A Phillips Norelco Schultz goniometer was used with a Phillips Norelco x-ray diffraction unit to obtain the diffracted x-ray intensity data from which the pole figures were plotted. The diffracted x-ray intensities from the sheet specimens were compared to the intensities from a standard copper specimen with no preferred orientation. This standard was made by lightly compacting copper powder in a press and annealing. Relative intensity values between the cold worked and recrystallized copper specimens could then be directly compared.

Testing Procedure

X-ray diffraction profiles were obtained from the fatigue specimens before and after the fatigue test using a Phillips Norelco x-ray diffraction unit to record the {111}, {200}, {222}, and {400} reflections

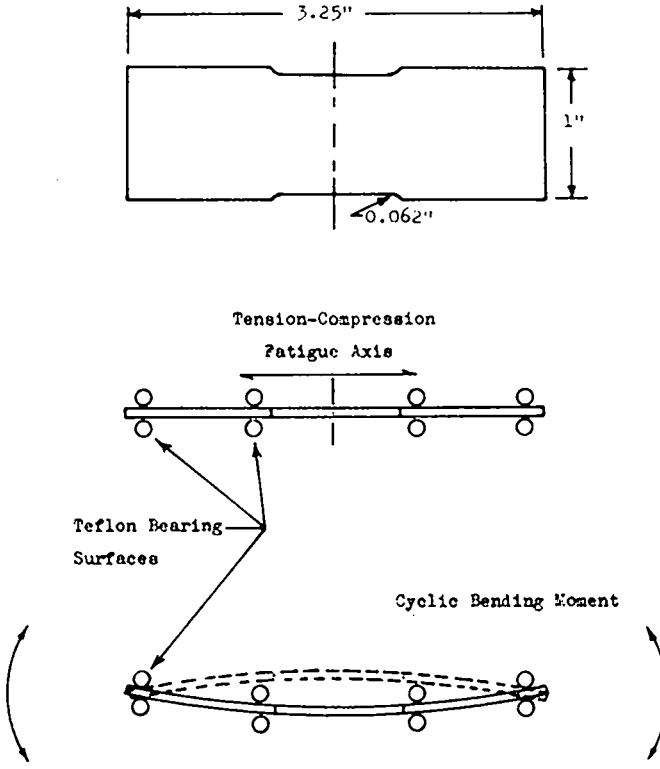

SPECIMEN CONFIGURATION FOR FATIGUE CYCLING

FIGURE 1

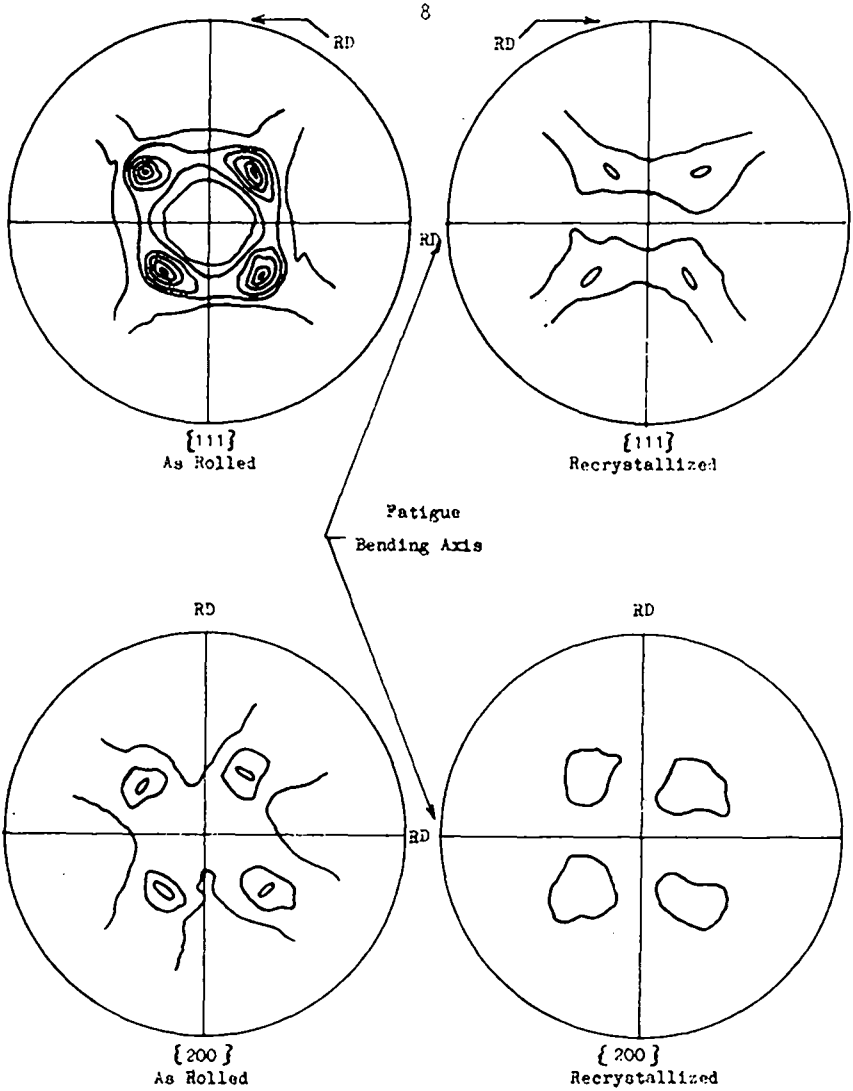

{111} AND {200} POLE FIGURES OF "AS ROLLED" AND RECRYSTALLIZED COPPER SHEET.

FIGURE 2

from the fatigue specimens on strip chart paper. A single tooth ratchet gear advanced the goniometer in steps of 0.01° 2θ for every revolution of the continuously rotating drive motor. Each revolution required approximately 30 seconds; hence, a statistical average of the intensity for each step could be obtained i.e. from 120 cps at background level to 1500 cps at the peak. (An automatic print out and step scanning unit was not available with the particular x-ray diffraction unit used.) A micro-switch which actuated a marker pen on the strip chart recorder was connected to the ratchet gear to give a reference pip for every incremental advance. The operating conditions for the x-ray diffraction unit are listed below.

Operating Conditions for Phillips Norelco X-ray Diffraction Unit

Copper x-ray tube 40 KV 20 ma.
Scintillation detector 1 KV
Phillips Norelco pulse height amplifier and discriminator

{111}, {200} Reflections	{222}, {400} Reflections
1° divergent slit	4° divergent slit
nickel filter	nickel filter
0.003" receiving slit	0.006" receiving slit
1° scatter slit	4° scatter slit

A commercial BUD fatigue machine was used to fatigue the specimens at a constant peak strain amplitude and a frequency of 1800 cpm. The specimens were loaded in four point reverse bending so that a zero average strain amplitude was maintained. The loading points were teflon bearings and their position with respect to the fatigue specimen is shown in Figure 1. The maximum peak strain amplitude could be varied by means of an adjustable cam and the progress of the fatigue test was checked by stopping the fatigue machine and examining the specimen visually. The criterion used for defining failure was the noticeable signs of a fatigue crack approximately 0.1" long. A curve relating the number of cycles to failure for a given fatigue strain amplitude was determined for the copper specimens and specific levels of strain amplitude were selected for x-ray analysis as indicated in Figure 3. The strain ampli-

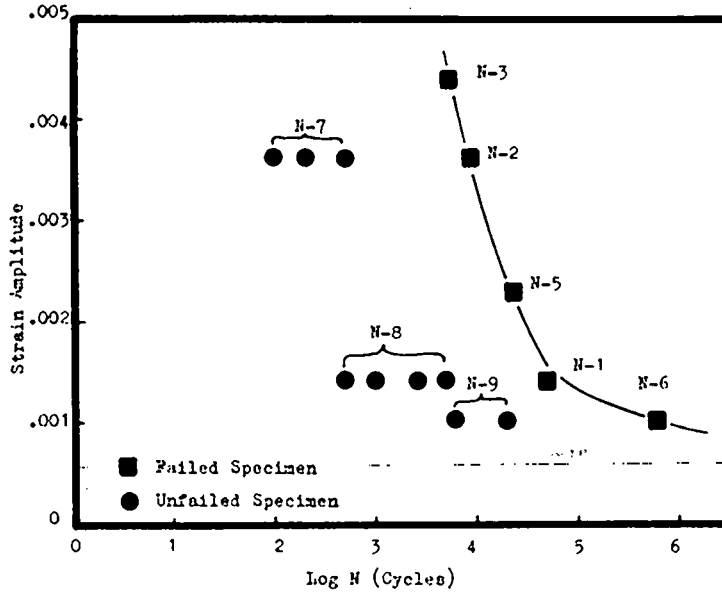

STRAIN AMPLITUDE OF FATIGUE PLOTTED
AS A FUNCTION OF FATIGUE CYCLES

FIGURE 3

tudes were measured with a strain gauge for various cam settings of the fatigue machine.

RESULTS

The diffracted x-ray intensity is read directly from the chart recording in increments of 0.01° 2θ. These readings are made as far out in the tails of the peak as is necessary to record the background intensity, normally to a distance of approximately five times the half peak width. The center of gravity of the peak is taken as the origin of the Fourier interval and this data (intensity for each 0.01° 2θ) transferred to IBM computer cards. The data is subsequently analyzed with a computer program which performs a Stokes analysis[16] on the cold worked and annealed peaks and gives directly the coefficients required. The annealed peak for each reflection was selected from the annealed peaks of all specimens and thereafter used as a standard.

The computer output data gives the sin and cos Fourier coefficents of the derived peak for increasing values of the harmonic number n, and averaging distance L. A typical set of curves showing the cos coefficient A_L as a function of L is presented in Figure 4 and the curves for all specimens are included in Appendix I.

Values of A_L for a unique L may then be determined and plotted in logarithmic form as a function of l_o^2. Theory[4] predicts that for various orders of the same reflection and also when isotropic strains and domain sizes are present, the resulting points for each L will lie on a straight line. For the special case of fatigue damage, $\ln A_L$ for $\{111\}$ and $\{222\}$ reflections fall consistantly above the straight line drawn through the $\{200\}$ and $\{400\}$ reflections. Assuming these grains can be treated independently, then the crystals oriented for $\{200\}$ - $\{400\}$ reflections indicate larger strains and larger coherently diffracting domain sizes than those crystals giving rise to $\{111\}$ and $\{222\}$ reflections.

The variation of $\ln A_L$ with l_o^2 for the $\langle 111 \rangle$ and $\langle 100 \rangle$ directions is shown in Figure 5. The rms strains and domain size coefficients are plotted in Figure 6 to represent the rms strain distribution and average coherently diffracting domain size in the crystals.

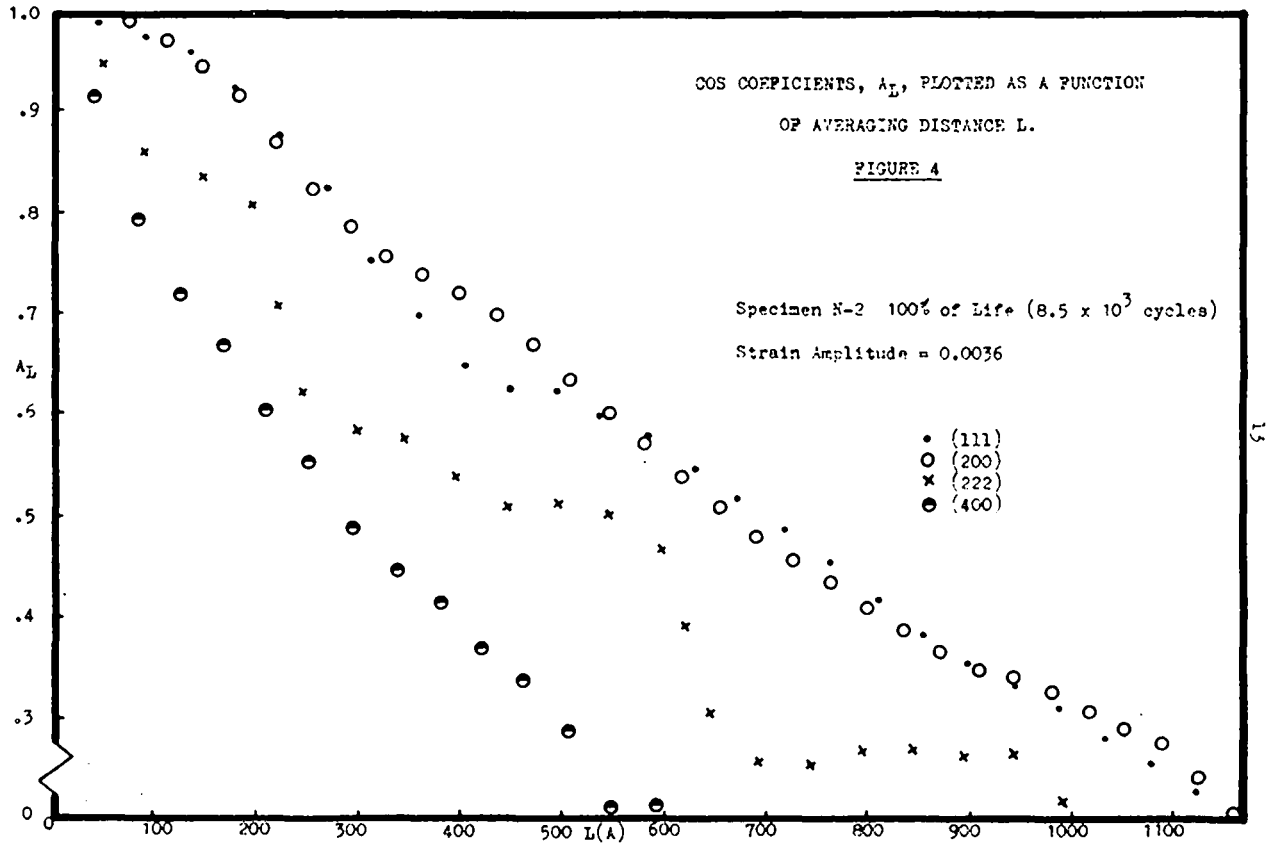
COS COEFICIENTS, A_L, PLOTTED AS A FUNCTION
OF AVERAGING DISTANCE L.
FIGURE 4
Specimen N-2 100% of Life (8.5 x 10^3 cycles)
Strain Amplitude = 0.0036
(111)
(200)
(222)
(400)
A_L
L(Å)
1.0
.9
.8
.7
.6
.5
.4
.3
0
100
200
300
400
500
600
700
800
900
1000
1100

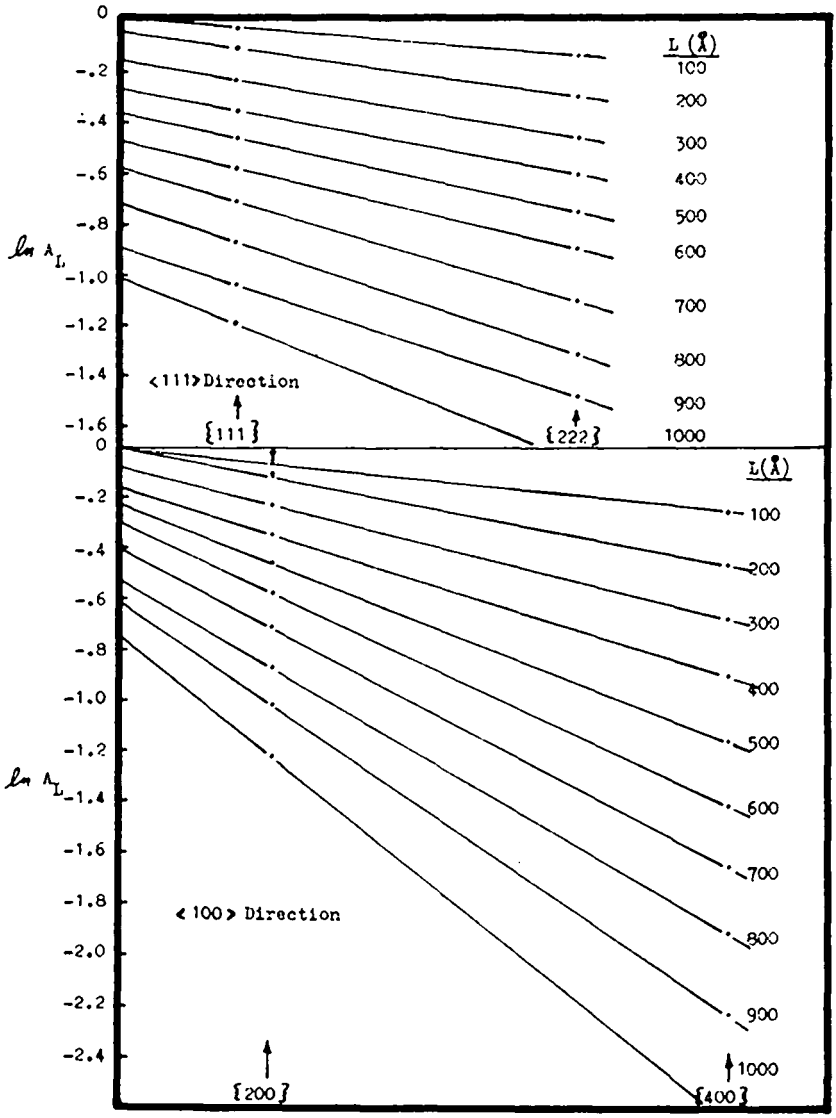

LOGARITHM OF THE COS COEFFICIENT, A_L, PLOTTED VS. ℓ_o^2 FOR THE <100> AND <111> DIRECTIONS.

FIGURE 5

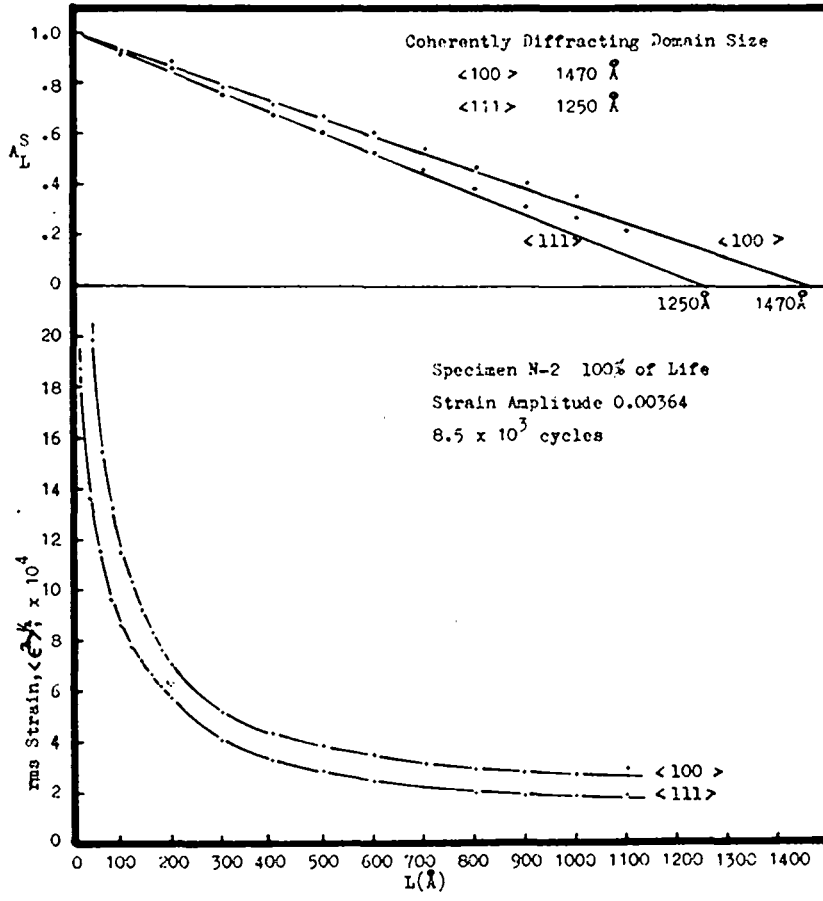

RMS STRAIN AS A FUNCTION OF AVERAGING DISTANCE, L, AND THE AVERAGE COHERENTLY DIFFRACTING DOMAIN SIZE FOR THE <100> AND <111> DIRECTIONS.

FIGURE 6

DISCUSSION OF RESULTS

The high degree of preferred orientation resulting from cross-rolling at room temperature was nearly eliminated during annealing as shown by the pole figures (c.f. Figure 2) although some traces of the original texture remained. The significance of Figure 2 is to show that the density of the <111> and <200> poles for corresponding positions of the pole figure is relatively the same i.e. they approximate the conditions defined by a randomly oriented collection of crystallites.

The state of crystalline perfection was well developed in the individual grains of annealed copper which resulted in a reduction of intensity by extinction. Although the intensity is reduced by this effect extinction per se has little influence on the line profile. If the ratio of observed intensity to theorectical intensity is used as a measure of extinction, then it can be shown[17-19] that for primay and secondary extinction appropriate corrections are given by the formulae:

Primay Extinction $$\frac{I_{obs.}}{I} = \left(\frac{f_{obs}}{f}\right)^2 = 1 - g f^2 K \qquad (11)$$

Secondary Extinction $$\frac{I_{obs}}{I} = \left(\frac{f_{obs}}{f}\right)^2 = 1 - \frac{g' f^2 K}{\sin 2\theta} \qquad (12)$$

where f = atomic scattering factor

g, g' = constants independent of the Bragg angle and dependent primarily on the dimensions and angular distributions of the coherently diffracting domains

K = polarization factor

The broadened x-ray lines from fatigued copper were sufficiently narrow ($\sim$0.5 degrees 2θ) to make the angular dependence of f, K and $\sin 2\theta$ essentially constant over the width of the line; hence, to a good approximation the theoretical intensity, when affected by extinction, is merely reduced by a constant factor which does not alter the shape or profile of the line.

Extinction may result in a secondary effect when an insufficient

number of grains are sampled to provide good statistical distribution of crystallite orientations. The purpose of selecting a representative annealed peak to be used as a standard was due to this reason. Slight inhomogeneities present in the annealed grains due to variations in orientation and substructure resulted in intensity fluctuations beneath an envelope representing the average over all of the specimen. Since fatigue at low strain amplitude levels leads to very slight broadening, these variations in the annealed specimens sometimes outweighed the average broadening effect. Thus, large scatter was observed at low strain amplitude levels. In retrospect, much of this problem seems to arise from extinction effects, which disapear abruptly for any degree of cold work. The annealed peaks therefore would be more susceptible to errors instead of the broadened peaks. This effect could have been minimized by using harder radiation and by oscillating the specimen to achieve better sampling of the crystallites.

The actual influence of this secondary extinction effect on the experimental results is to produce either 1) an annealed peak which is too broad or 2) an annealed peak which is too narrow. It can easily be shown that if the annealed peak is "too broad", apparent larger rms strains and larger coherently diffracting domain sizes would be determined whereas if the annealed peak is "too narrow", apparent smaller rms strains and smaller coherently diffracting domain sizes would be determined. The domain sizes which were measured did not vary in a systematic way with fatigue life or increasing strain amplitude and typical values ranged between 1000 and 3000 angstroms. Domain sizes of this magnitude result in very little broadening and hence the analysis is subject to considerable errors. Therefore no further mention will be made in the ensuing discussion on coherently diffracting domain sizes as determined by the Warren-Averbach analysis. On the other hand the rms strains were seen to vary systematically with fatigue life and increasing strain amplitude. The absolute values of the rms strains are somewhat uncertain, however their relative changes with averaging distance and strain amplitude, and their insensitivity to duration of testing is well extablished.

A major difficulty in analyzing the broadening function was due

to the fluctuations present in the curves relating the cos coefficients, A_L, to the averaging distance L (c.f. Figure 4 and Appendix I). Fluctuations present in these curves may be due to 1) data points inadequately defined in the tails of the diffraction peak and 2) the asymmetry of the annealing peak due to extinction and other effects mentioned above, when these effects are not carried over into the broadened peaks. Large sin coefficients are introduced when the asymmetries are in one peak only and it is easily shown that this in turn leads to fluctuations in the cos coefficients. If the background level is not determined correctly errors will be introduced near the small A_L region of the A_L vs. L curve. These errors represent a significant part of the broadening function when the profiles of the annealed peak and cold worked peak are very similar.

The use of plane bulk specimens for this investigation limited the analysis in the sense that any diffraction geometry satisfying the Bragg conditions of equal angles between incident and diffracted beams and the specimen's surface selectively determines which crystallites will contribute to the reflection. One set of crystals will give rise to {111} - {222} reflections and a completely different set will result in {200} - {400} reflections, and these different sets of crystals are necessarily affected differently by the experimentally imposed strains. This necessitates a certain degree of caution when comparing the rms strains between the <100> and <111> directions.

The strain amplitudes used for these fatigue tests represents shear stresses slightly larger than the yield stress of copper. Hence deformaion would be expected to be more severe in those grains oriented for high resolved shear stress. The range of orientations of tension-compression fatigue axes (c.f. Figure 1) sampled by our x-ray geometry for the {111} - {222} and {200} - {400} reflections are indicated on the stereographic triangle in Figure 7a. These are superimposed on equal Schmid factor contours. The approximation that only uniaxial fatigue stresses are present in the crystallites being examined is reasonable since the x-ray data is more representative of the layers in the surface than those in the interior i.e. 50% of the diffracted intensity comes from a volume 0.00015 inches in depth while 99% of the intensity comes from a volume 0.0008 inches in depth. Hence we are

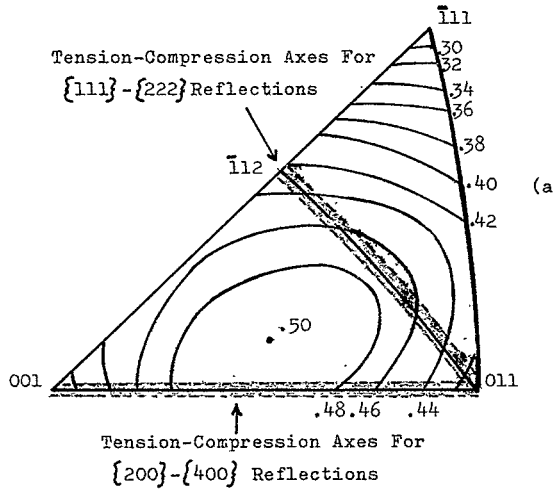

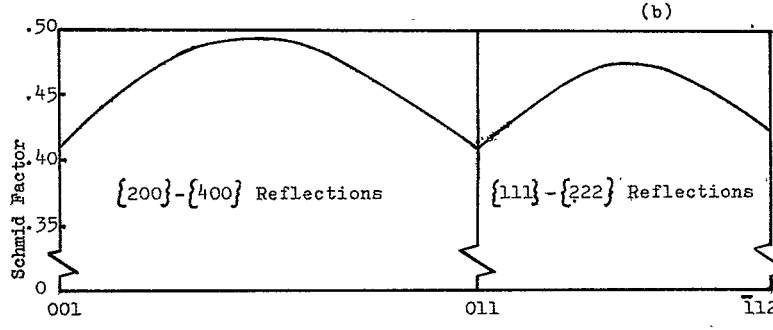

THE RANGE OF ORIENTATIONS OF TENSION-COMPRESSION FATIGUE AXES FOR ALL OF THE GRAINS CONTRIBUTING TO BOTH THE {111} AND {200} REFLECTIONS SUPERIMPOSED ON CONTOURS OF EQUAL SCHMID FACTORS FOR THE [110] - (111) SLIP SYSTEMS.

FIGURE 7

effectively examining only the crystallites in the surface grains since the annealed grain size is approximately 0.0004 inches. From Figure 7b, therefore, the crystallites having the largest values of Schmid factors will be those which contribute to the {200} -{400} reflections; and probably more important with respect to fatigue hardening is the fact that these grains are oriented for duplex slip. The {111} - {222} type grains on the other hand have smaller Schmid factors and are oriented for single slip. It would be expected therefore that the {200} - {400} type grains would undergo a greater degree of hardening and result in more dislocation interactions.

The rms strains determined in the x-ray analysis can be more appropriately discussed by referring to the stereographic projection in Figure 8. The {200} - {400} grains will deform by slip on $(\bar{1}11)$ and (111) planes in the [101] and $[\bar{1}01]$ directions respectively whereas the {111} - {222} grains will deform by slip on the (111) plane in the $[\bar{1}01]$direction. Since the rms strains are measured in directions normal to the diffracting planes, the $[\bar{1}00]$ and $[1\bar{1}1]$ directions refer to the normals of the {200} - {400} and {111} - {222} type grains. Therefore as a first approximation the component of strain normal to the $(\bar{1}00)$ diffraction planes is $\sqrt{2}/2$ rms strain while that normal to the $(1\bar{1}1)$ diffraction planes is 0.0 rms strain. Hence from this overly simplified model of dislocation interactions one would expect larger rms strains to be measured with the $(\bar{1}00)$ reflections.

The elimination of extinction effects with fatigue is a direct indication of the change in coherency length with deformation. From the following table it is easily seen that the {200} reflections appear to be more affected than the {111} reflections as a result of increasing strain amplitude of fatigue.

PERCENT INCREASE IN INTEGRATED INTENSITY WITH FATIGUE

Strain Amplitude	{111}	{200}
0.00105	30%	71%
0.00145	28%	184%
0.00273	51%	114%
0.00364	107%	91%
0.00442	129%	222%

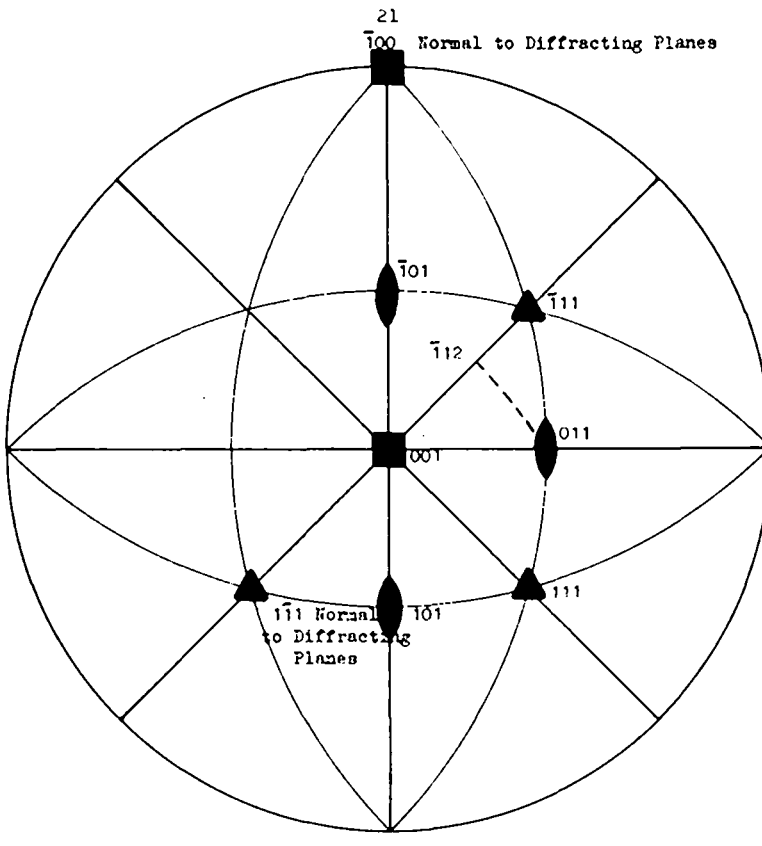

STEREOGRAPHIC PROJECTION SHOWING CRYSTALLOGRAPHIC SLIP PLANES AND SLIP DIRECTIONS FOR CRYSTALS ORIENTED FOR $(\bar{1}00)$ and $(1\bar{1}1)$ REFLECTIONS.

FIGURE 8

Assuming that the specimen which exhibits the largest increase in integrated intensity represents an ideal mosaic, and that primary extinction is affecting the annealed reflections, the size of the individual mosaic crystallites prior to fatigue damage can be estimated[19]. For the case where the intensity of the fatigued specimen increased by 222%, the annealed mosaic crystallite size is $\sim 1\mu$. The smaller percentage increases in integrated intensity, therefore, represent the situation where fatigue damage has not entirely eliminated the large coherent domains responsible for extinction.

Saturation of the rms strain occurs at an extremely early stage in the fatigue life of copper. There is some indication it reaches saturation within the first 2% of the life. The rms strain averaged over 100, 500, and 1000 angstroms for various fractions of the fatigue life are shown in Figures 9, 10, and 11. The early saturation of rms strain is consistent with other investigations[20,21] and with a recent theory of fatigue hardening in high stacking fault energy metals[22]. The rapid hardening stage is based on the premise that the rate of hardening is dependent on the rate of formation of debris obstacles in the active slip planes where the debris obstacles are taken to include prismatic dislocation loops formed by cross-slip of jogged screw dislocations and also point defect aggregates. The rate is thus dependent on the ease of cross-slip or stacking fault energy. It has been shown[22] that the initial rate of hardening in copper single crystals is temperature dependent, the rate increasing with increasing temperature, in a way which suggests enhanced cross-slip by thermal activation. Saturation of the rms strain therefore occurs when the individual dislocations are trapped by the debris collecting in the slip planes and when the back stresses increase to the point where the dislocation sources can no longer operate. It has been proposed that the majority of the strain during subsequent fatigue is then accomodated by the flip-flop of the dislocation dipoles from one equilibrium position to another i.e. from an orientation of 45° to 135°. This mechanism would also explain the hysteresis loop observed during tension-compression fatigue tests. A small percentage of the fatigue strain could be taken up by the bowing out of dislocations but this would not result in a hysteresis curve in FCC crystals. The density and size of prismatic disloc-

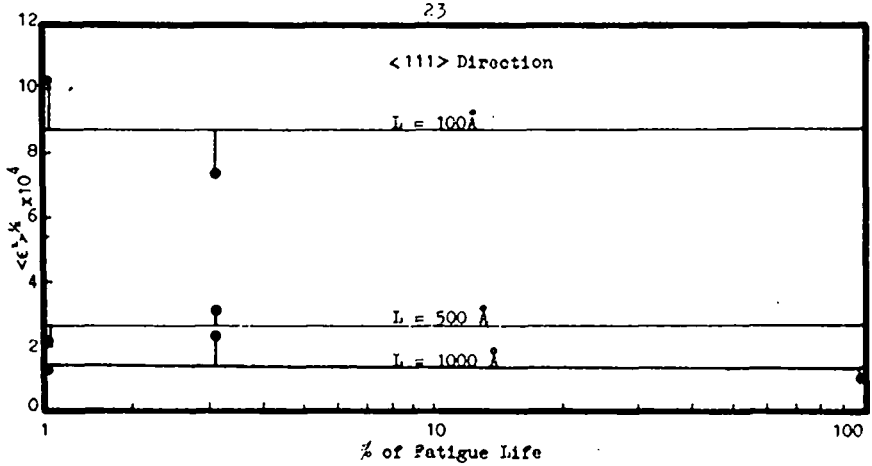

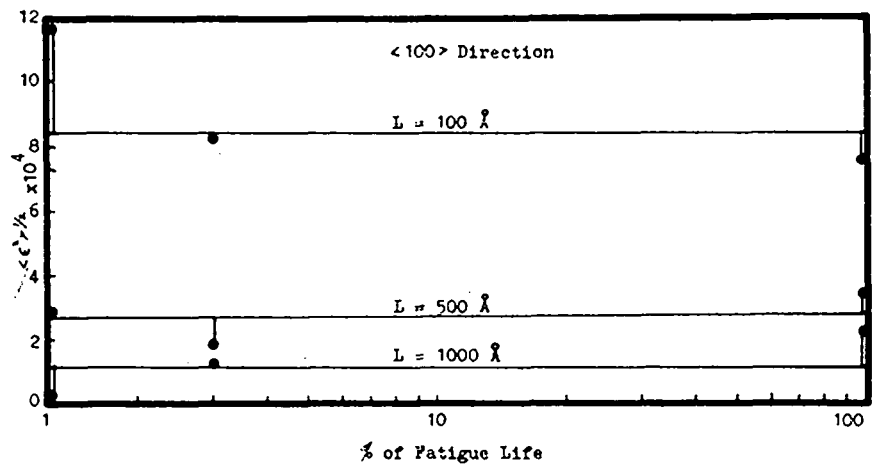

RMS STRAINS AVERAGED OVER 100, 500, AND 1000 ANGSTROM DISTANCES AS A FUNCTION OF PATIGUE LIFE.
(Strain Amplitude 0.00105, 5.71×10^5 Cycles to Failure)

FIGURE 9

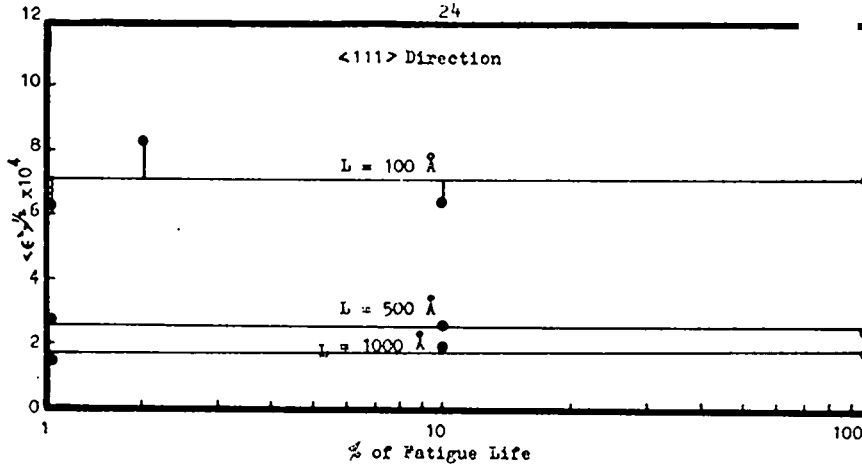

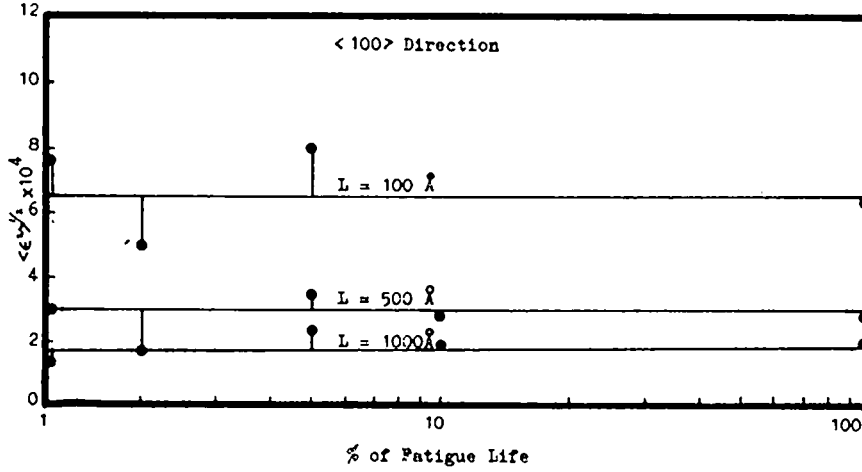

RMS STRAINS AVERAGED OVER 100, 500, AND 1000 ANGSTROM DISTANCES AS A FUNCTION OF FATIGUE LIFE.
(Strain Amplitude 0.00145, 4.84×10^4 Cycles to Failure)

FIGURE 10

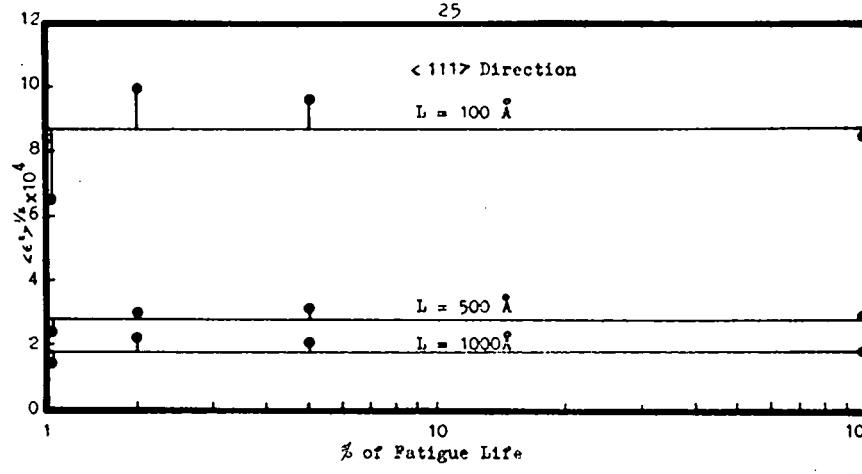

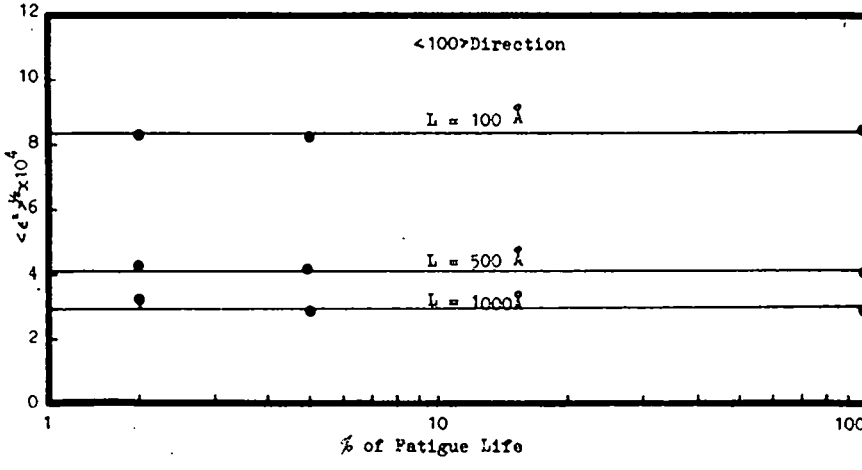

RMS STRAINS AVERAGED OVER 100, 500, AND 1000 ANGSTROM DISTANCES AS A FUNCTION OF PATIGUE LIFE.
(Strain Amplitude 0.00364, 8.5 x 10^3 Cycles to Failure)

FIGURE 11

ation loops required to accomodate the strain during a normal fatigue test is consistent with the dislocation arrangements which are observed. The dislocation loop densities in the dense clusters are approximately 10^{10} - 10^{11} loop dislocations per square centimeter. This dislocation density, if not in the form of dipoles, would normally result in severely broadened x-ray diffraction lines, but because of the opposite signs of the Burgers vectors in the dipoles their strain fields tend to cancel producing a minimum degree of broadening and the resultant small values of rms strain.

The effect of increasing strain amplitude of fatigue on the rms strains (averaged over 100, 500, and 1000 angstrom distances) in the <100> and <111> directions is illustrated in Figure 12. The increase of rms strains with increasing strain amplitude of fatigue becomes larger as the averaging distance decreases. This would imply that more short range interactions are occurring between dislocations as a result of increased strain amplitude and that these are not significantly affecting the total rms strains at large distances. Either an increased dislocation dipole density or larger numbers of single dislocations could produce this effect. If more single dislocations were being introduced as the strain amplitude increased, the transition observed in the dislocation arrangements between low and high strain amplitude fatigue could be explained i.e. a definite cell structure develops during high strain fatigue which resembles the cell structure produced during uniaxial tension. The single dislocations could result in sufficient strain energy to form the cell structure and also to cause recrystallization of the material on annealing; material fatigued at low strain amplitude does not recrystallize with annealing.

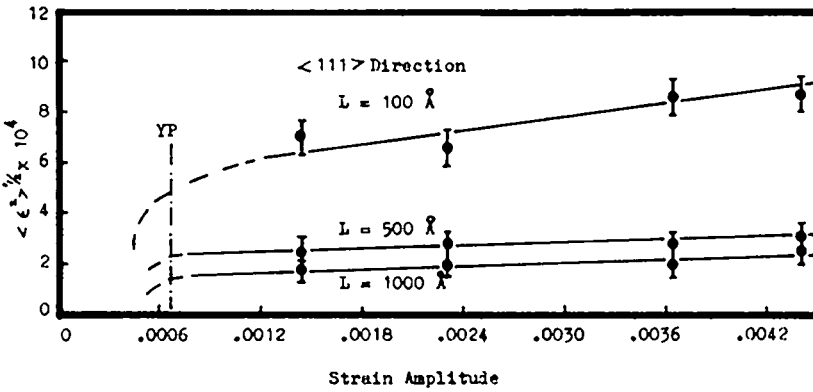

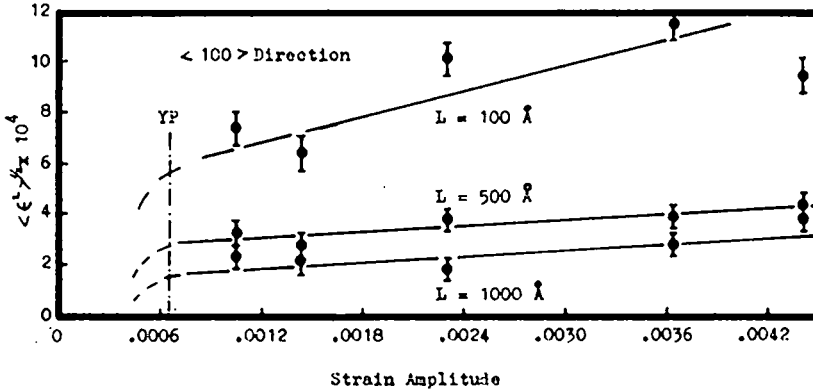

RMS STRAINS AVERAGED OVER 100, 500, AND 1000 ANGSTROM DISTANCES AS A FUNCTION OF STRAIN AMPLITUDE

FIGURE 12

CONCLUSIONS

1. Saturation of the rapid hardening stage occurs within the first 2% of the fatigue life in copper.

2. Small values of rms strains averaged over distances above 100 angstroms are found in fatigued copper which is a direct consequence of the short range strains associated with the clusters of dipoles produced during fatigue.

3. The conclusions arrived at in this investigation can be explained by the dislocation arrangements which are observed by transmission electron microscopy if it is assumed that the surface damage observed by x-ray diffraction is typical of the damage in the interior which is examined by transmission electron microscopy.

RECOMMENDATIONS FOR FUTURE RESEARCH

1. The fatigue specimens should be electropolished to various depths below the surface after fatigue to see if the measured properties differ and to obtain an idea of the processes occurring in the interior of the specimen.

2. Metals having much lower stacking fault energies should be investigated by means of this technique to see if there is a difference in measured properties with stacking fault energy in a way which is consistent with observations by transmission electron microscopy and theory.

Improvements could be made in the experimental procedure by the following:

1. Improved counting statistics by automatic step scanning and digital print-out.

2. Crystal monochromated x-radiation to provide decreased line widths and lower background levels.

3. Simple oscillation or rotation of specimen to improve sampling statistics.

4. The fatigue specimen configuration might be changed to a small diameter cylinder prepared from a single crystal having a <110> direction parallel to the specimen length so that the {111} - {222} and {200}-{400} reflections could be collected from the same crystal in order to give a direct comparison of the measured properties in the two directions. This would necessitate a tension-compression fatigue machine.

5. The use of shorter wave length x-rays would attain a greater depth of penetration and therefore increased volume of material would be examined. However certain difficulties might be encountered by this approach due to the narrow line width which would result i.e. the broadening function would also be reduced in width and might result in increased errors of measurement.

REFERENCES

1. Warren, Averbach, J. App. Phys. 21, 595,(1950)
2. Warren, Averbach, ibid. 23, 497, (1952)
3. Warren, Averbach, ibid. 23, 1059, (1952)
4. Warren, Prog. Met. Phys. 8, 147, (1959)
5. N. Thompson, N. Wadsworth, Advanc. Phys. 7,72, (1958)
6. S. Moll, PHD Thesis, MIT (1959)
7. R. Hartmann, E. Macherauch, Z. Metallkde. 54, 197, (1963)
8. J. Friedel, Dislocations, 158, (1964) Addison-Wesley
9. D. Avery, W. Backofen, Acta. Met. 11, 795, (1963)
10. J. Robinson, J. Grosskreutz, Acta. Met. 11, 795, (1963)
11. R.M.N. Pelloux, Boeing Scientific Research Laboratories Document D1-82-0304, (1963)
12. R. Segall et. al., Phil. Mag. 6, 1493, (1961)
13. J. Grosskreutz, G. Shaw, Phil. Mag. 9, 961, (1964)
14. A. Lawley et. al., ARL 65-11, (1965)
15. R. Segall et. al., Electron Microscopy And Strength Of Crystals, 515, (1963) Interscience
16. A. Stokes, Proc. Phys. Soc. 61, 382, (1948)
17. A. Lang, Proc. Phys. Soc. 66, 1003, (1953)
18. G. Williams, R. Smallman, Proc. Phys. Soc. 68, 577, (1955)
19. S. Chandrasekhar, Adv. Phys. 9, 363, (1960)
20. W. Wood, R. Segall, Proc. Roy. Soc. 242, 180, (1952)
21. N. Wadsworth, Acta. Met. 11, 663, (1963)
22. C. Feltner, Phil. Mag. 12, 1229, (1965)

APPENDIX I

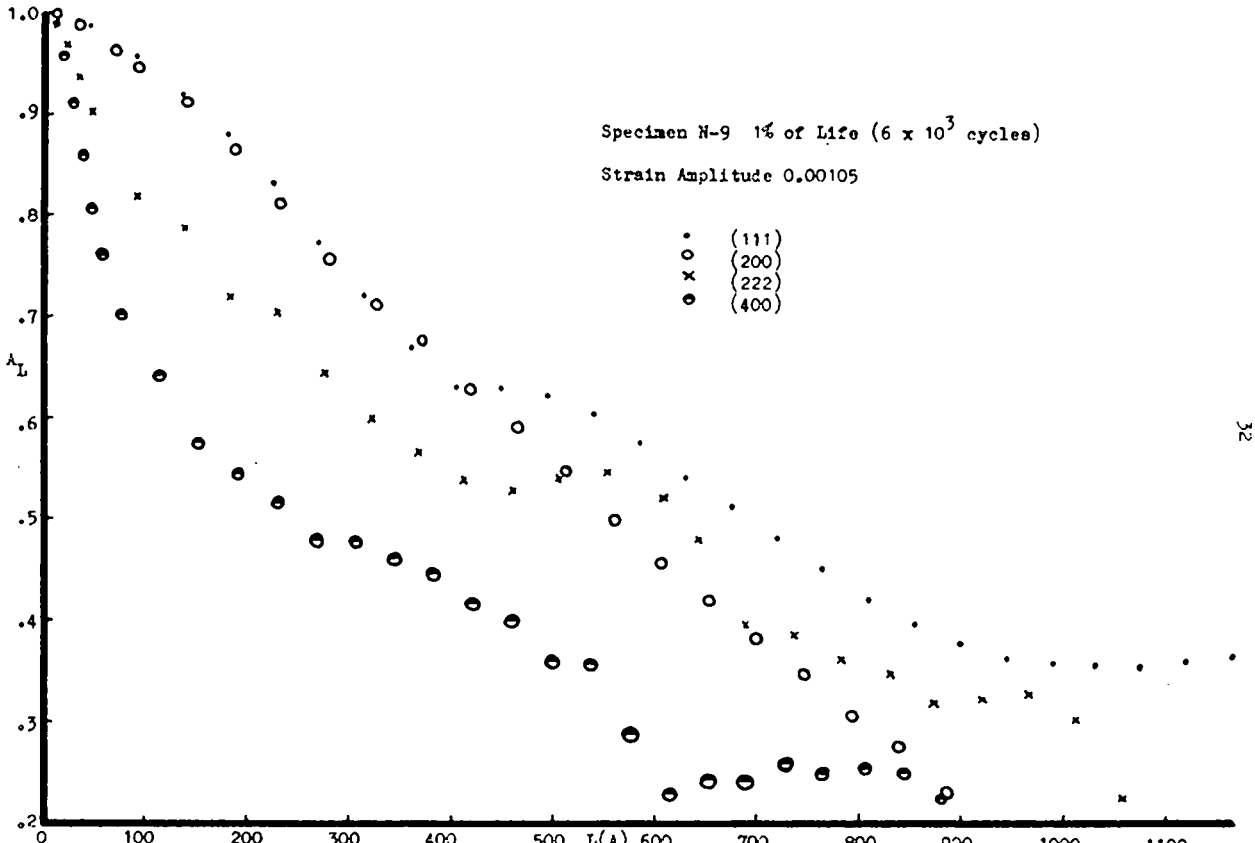
Specimen N-9 1% of Life (6 x 10^3 cycles)
Strain Amplitude 0.00105
(111)
(200)
(222)
(400)
A_L
L(A)
1.0
.9
.8
.7
.6
.5
.4
.3
.2
0
100
200
300
400
500
600
700
800
900
1000
1100

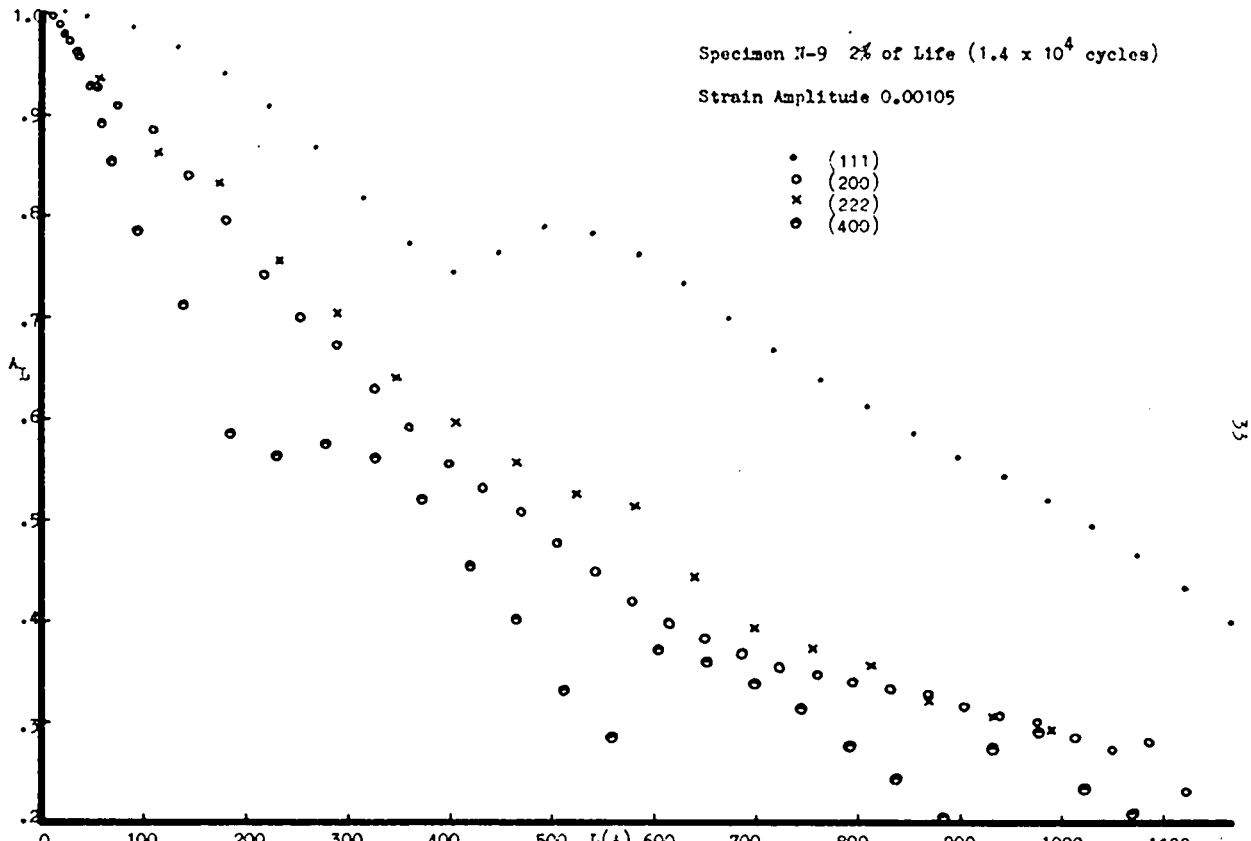
Specimen N-9 2% of Life (1.4 x 10^4 cycles)
Strain Amplitude 0.00105
(111)
(200)
(222)
(400)
A_L
1.0
.9
.8
.7
.6
.5
.4
.3
.2
0
100
200
300
400
500
L(Å)
600
700
800
900
1000
1100

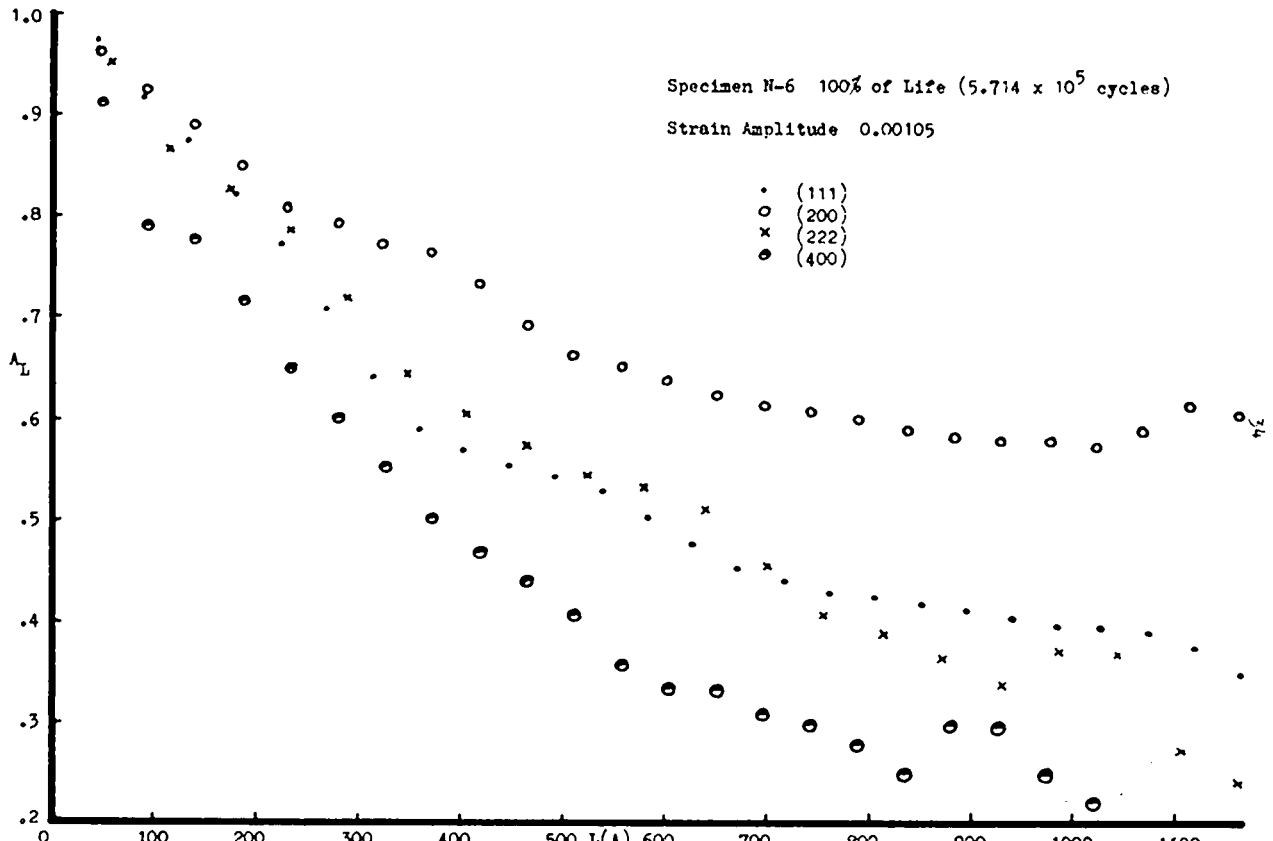
Specimen N-6 100% of Life (5.714 x 10^5 cycles)
Strain Amplitude 0.00105
(111)
(200)
(222)
(400)
A_L
1.0
.9
.8
.7
.6
.5
.4
.3
.2
0
100
200
300
400
500 L(Å) 600
700
800
900
1000
1100

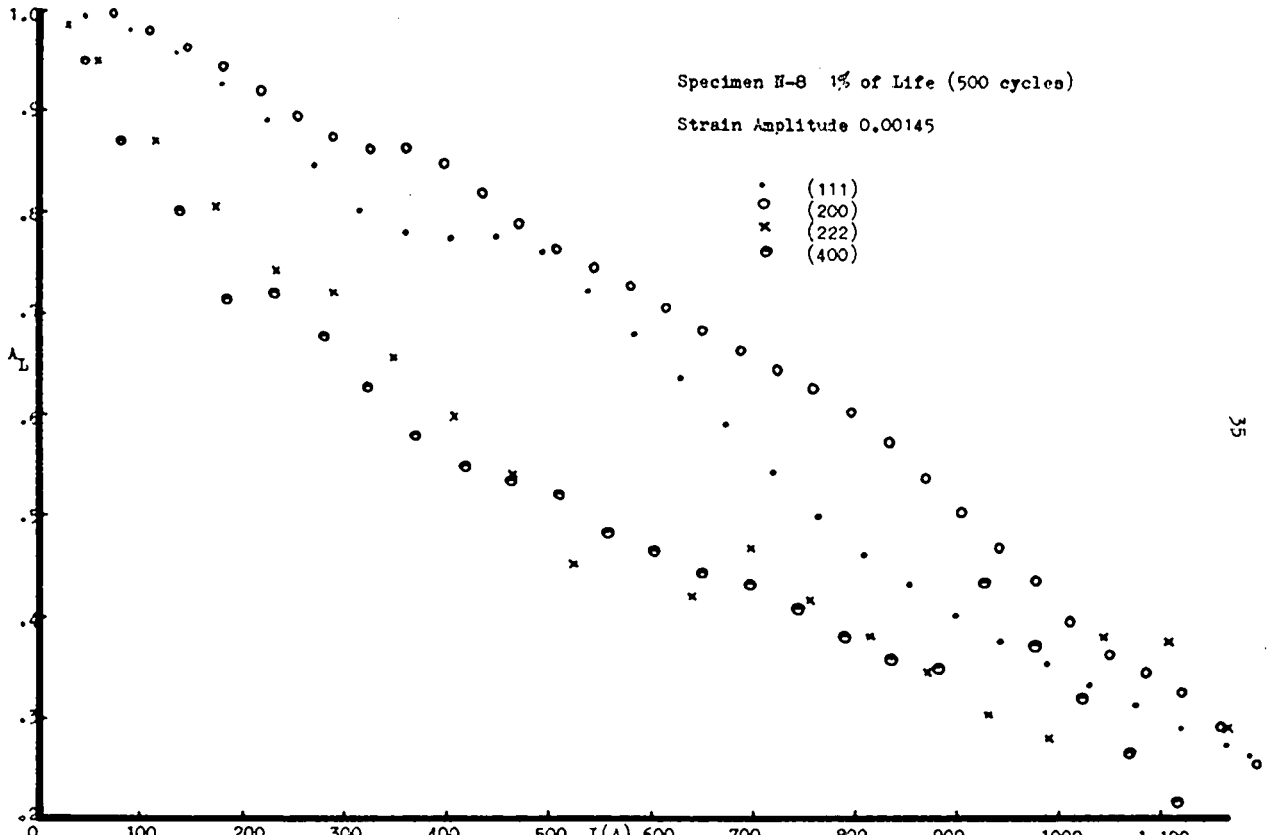
Specimen H-8 1% of Life (500 cycles)
Strain Amplitude 0.00145
(111)
(200)
(222)
(400)
A_L
1.0
.9
.8
.7
.6
.5
.4
.3
.2
0
100
200
300
400
500
L(A)
600
700
800
900
1000
1 100

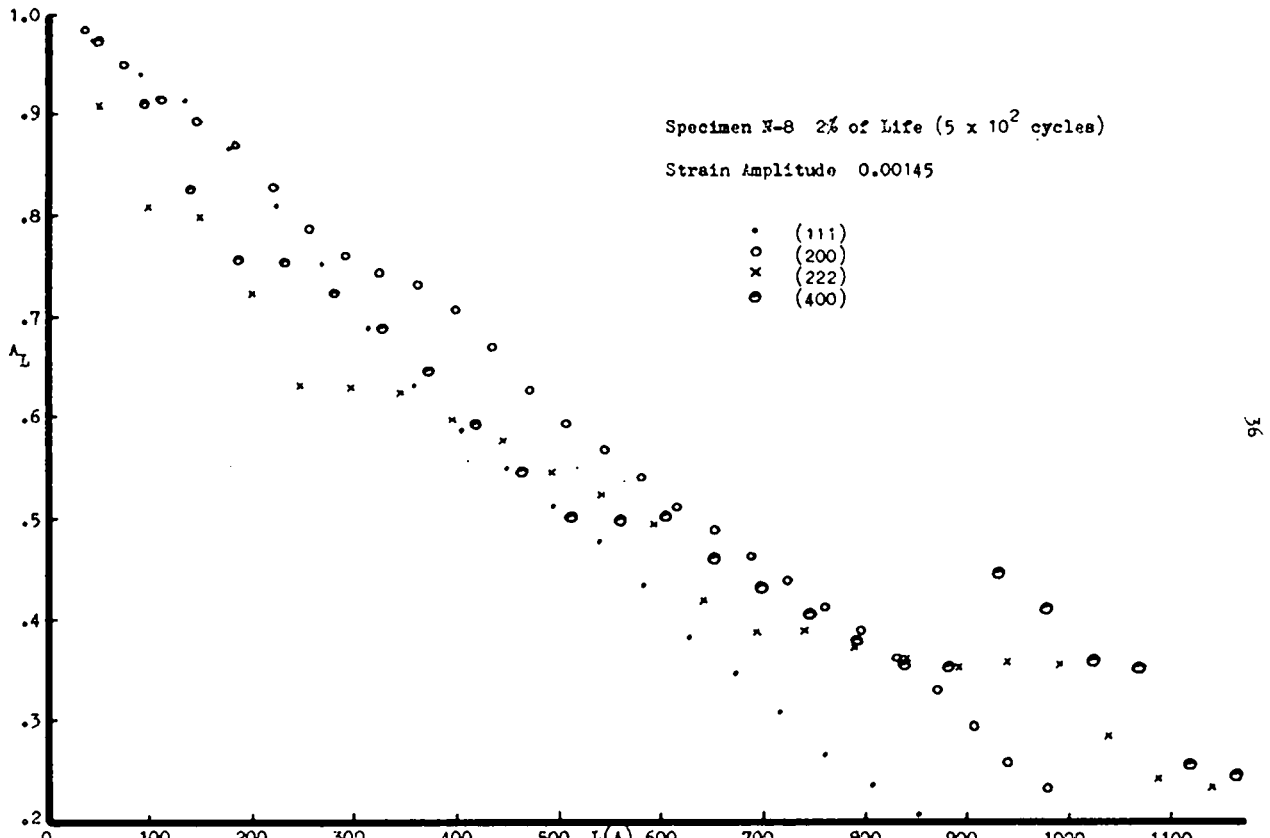
Specimen N-8 2% of Life (5 x 10^2 cycles)
Strain Amplitude 0.00145
(111)
(200)
(222)
(400)
A_L
L(A)
1.0
.9
.8
.7
.6
.5
.4
.3
.2
0
100
200
300
400
500
600
700
800
900
1000
1100

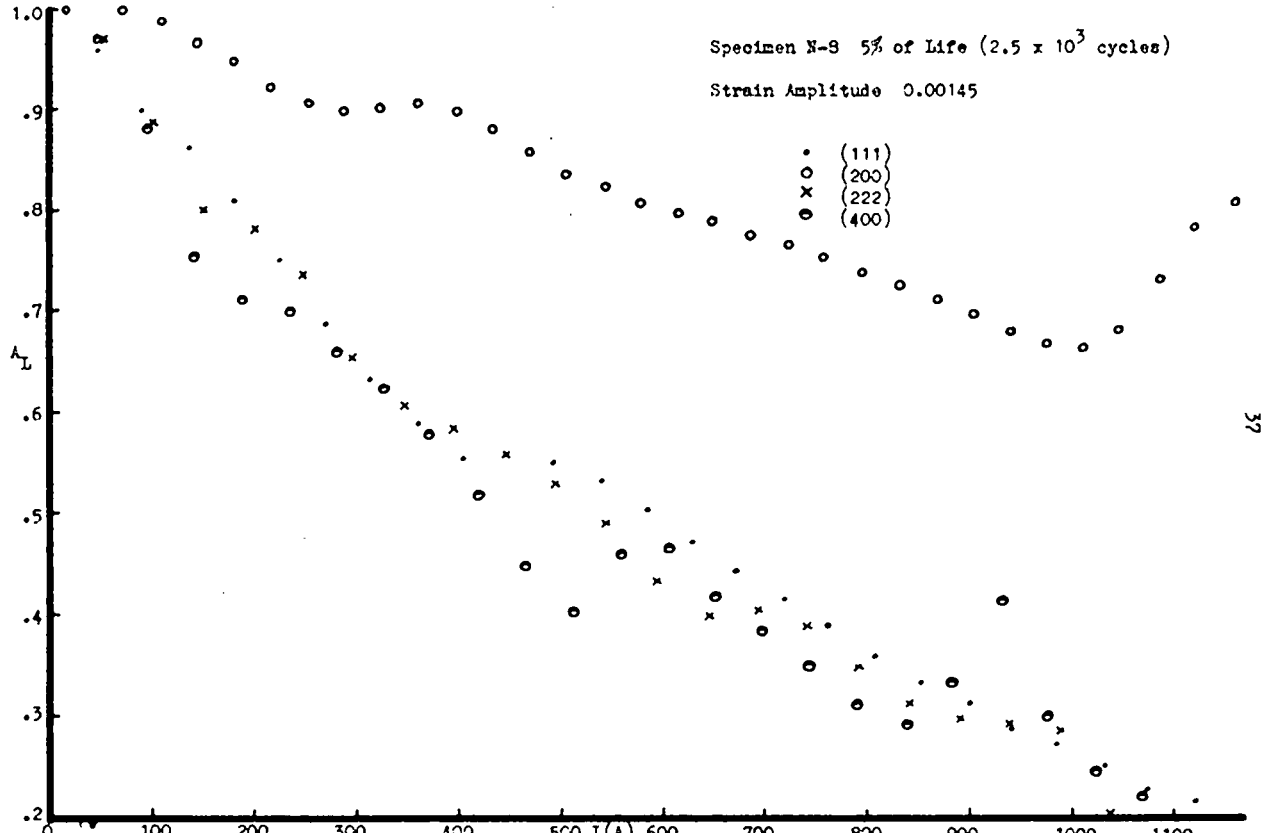
Specimen N-8 5% of Life (2.5 x 10^3 cycles)
Strain Amplitude 0.00145
(111)
(200)
(222)
(400)
A_L
1.0
.9
.8
.7
.6
.5
.4
.3
.2
0
100
200
300
400
500 L(A)
600
700
800
900
1000
1100

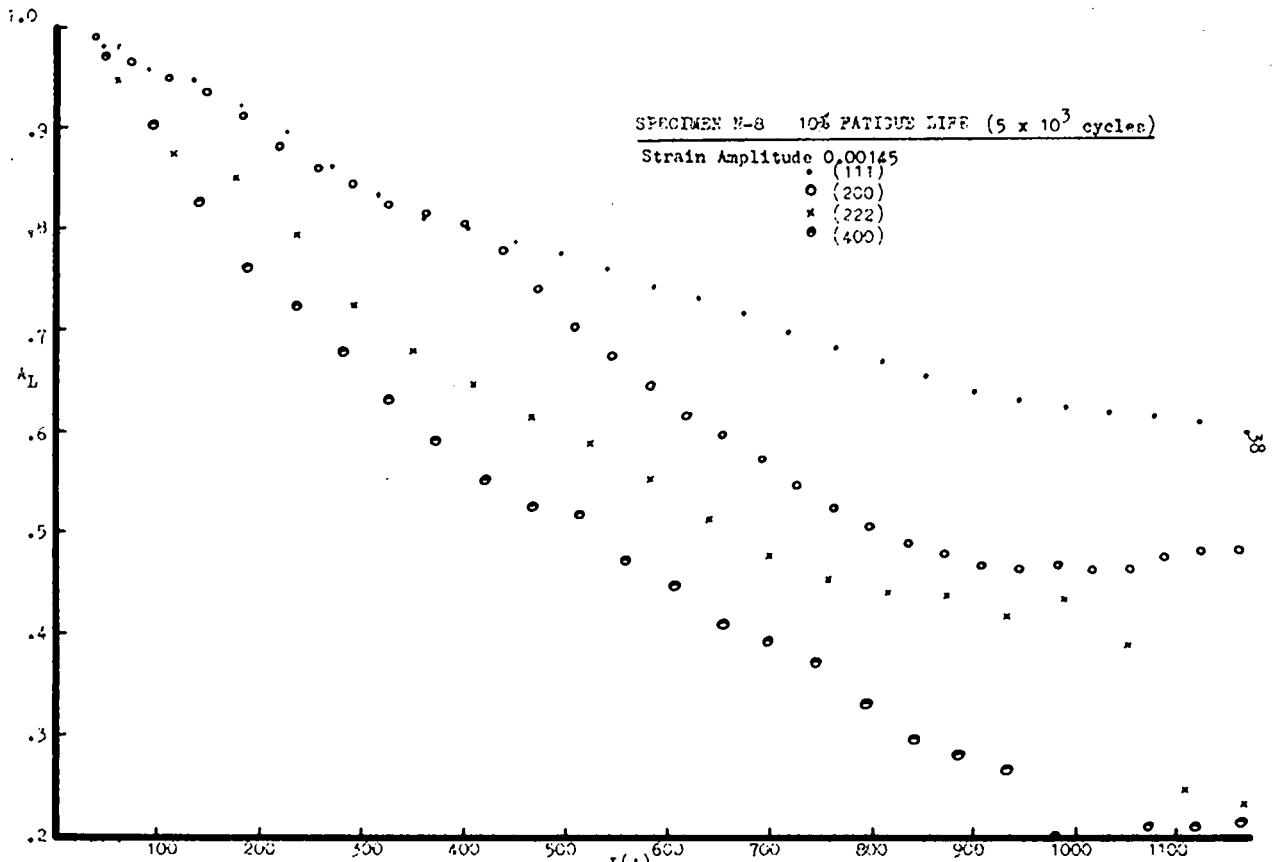
SPECIMEN M-8 10% FATIGUE LIFE (5 x 10^3 cycles)
Strain Amplitude 0.00145
(111)
(200)
(222)
(400)
1.0
.9
.8
.7
.6
.5
.4
.3
.2
A_L
100
200
300
400
500
600
700
800
900
1000
1100
L(A)

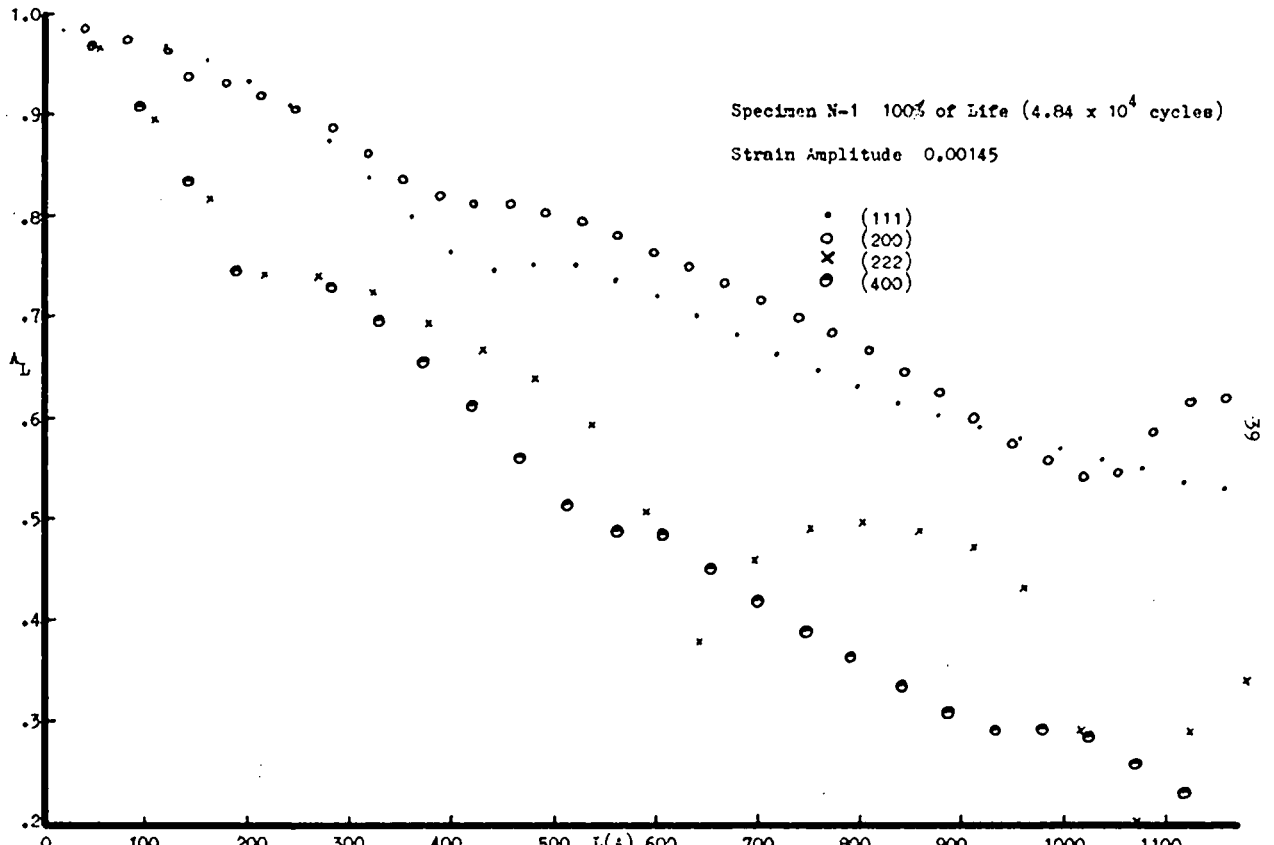
Specimen N-1 100% of Life (4.84 x 10^4 cycles)
Strain Amplitude 0.00145
(111)
(200)
(222)
(400)
A_L
L(A)
1.0
.9
.8
.7
.6
.5
.4
.3
.2
0
100
200
300
400
500
600
700
800
900
1000
1100

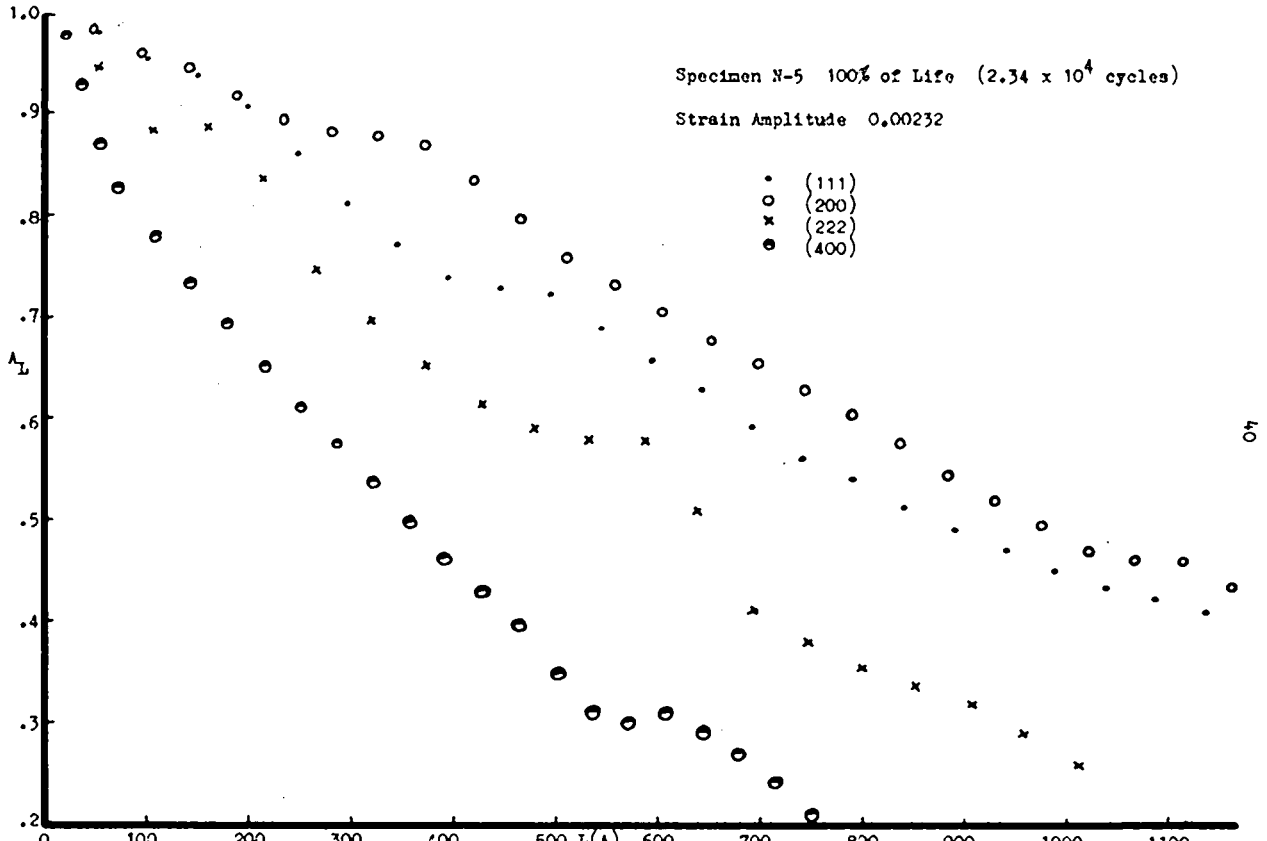
Specimen N-5 100% of Life (2.34 x 10^4 cycles)
Strain Amplitude 0.00232
(111)
(200)
(222)
(400)
A_L
L(A)
1.0
.9
.8
.7
.6
.5
.4
.3
.2
0
100
200
300
400
500
600
700
800
900
1000
1100

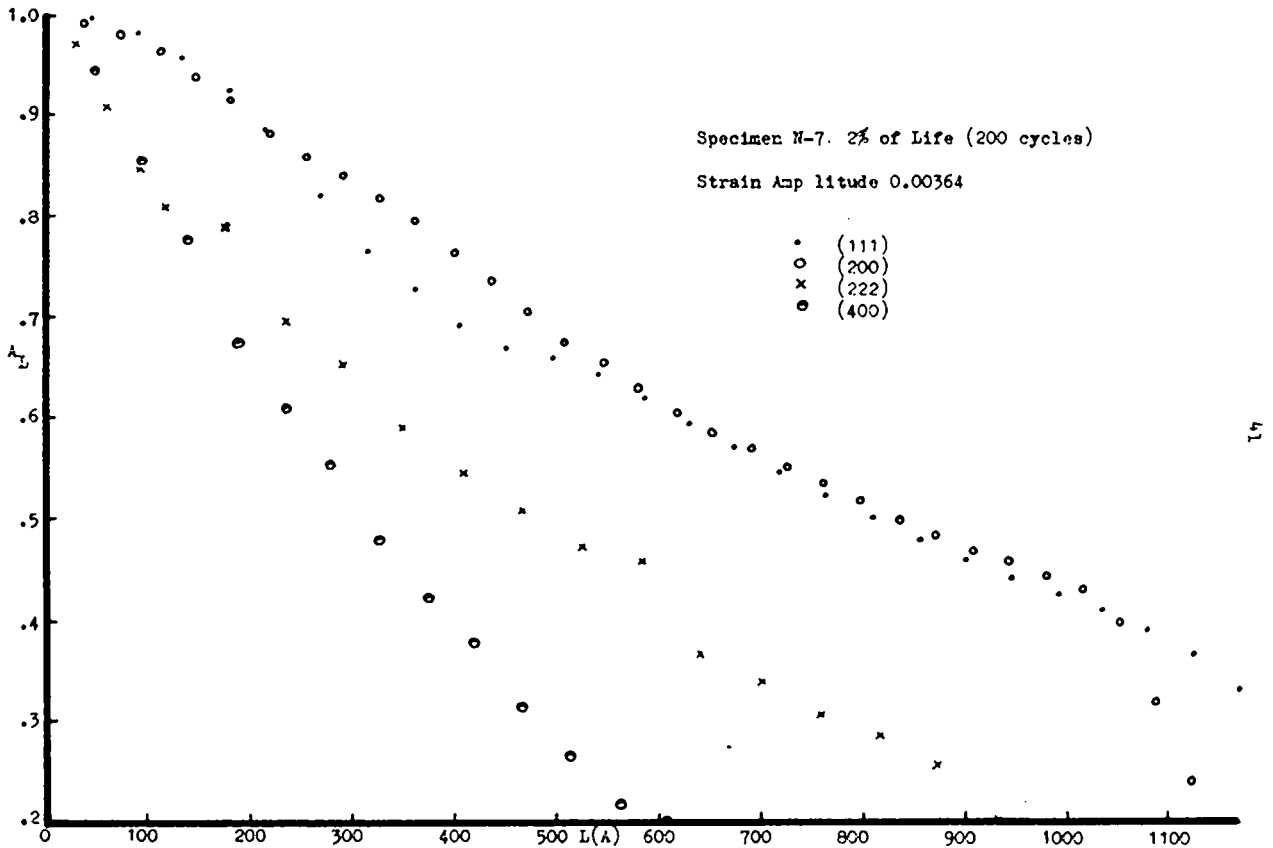
Specimen N-7. 2% of Life (200 cycles)
Strain Amplitude 0.00364
(111)
(200)
(222)
(400)
1.0
.9
.8
.7
.6
.5
.4
.3
.2
0
100
200
300
400
500
600
700
800
900
1000
1100
L(A)

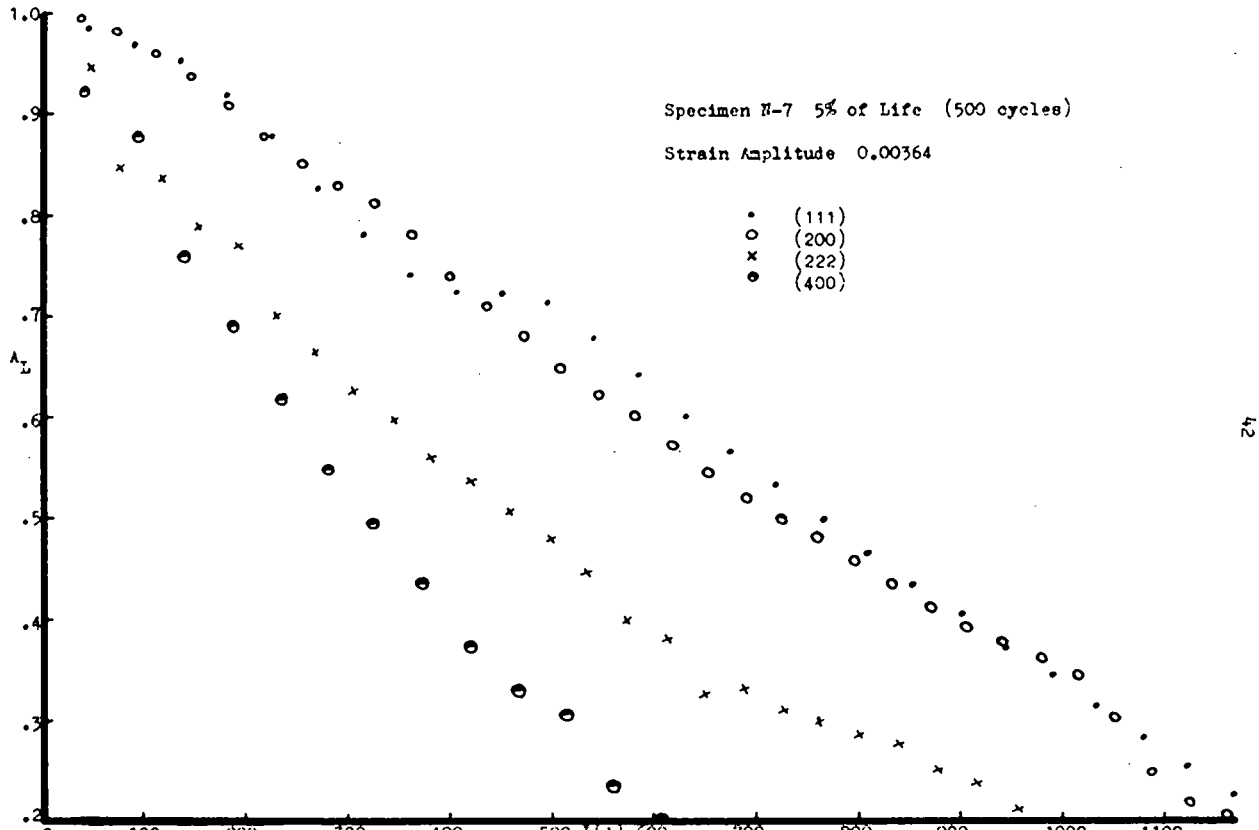
Specimen M-7 5% of Life (500 cycles)
Strain Amplitude 0.00364
(111)
(200)
(222)
(400)
A_L
1.0
.9
.8
.7
.6
.5
.4
.3
.2
0
100
200
300
400
500 L(λ) 600
700
800
900
1000
1100

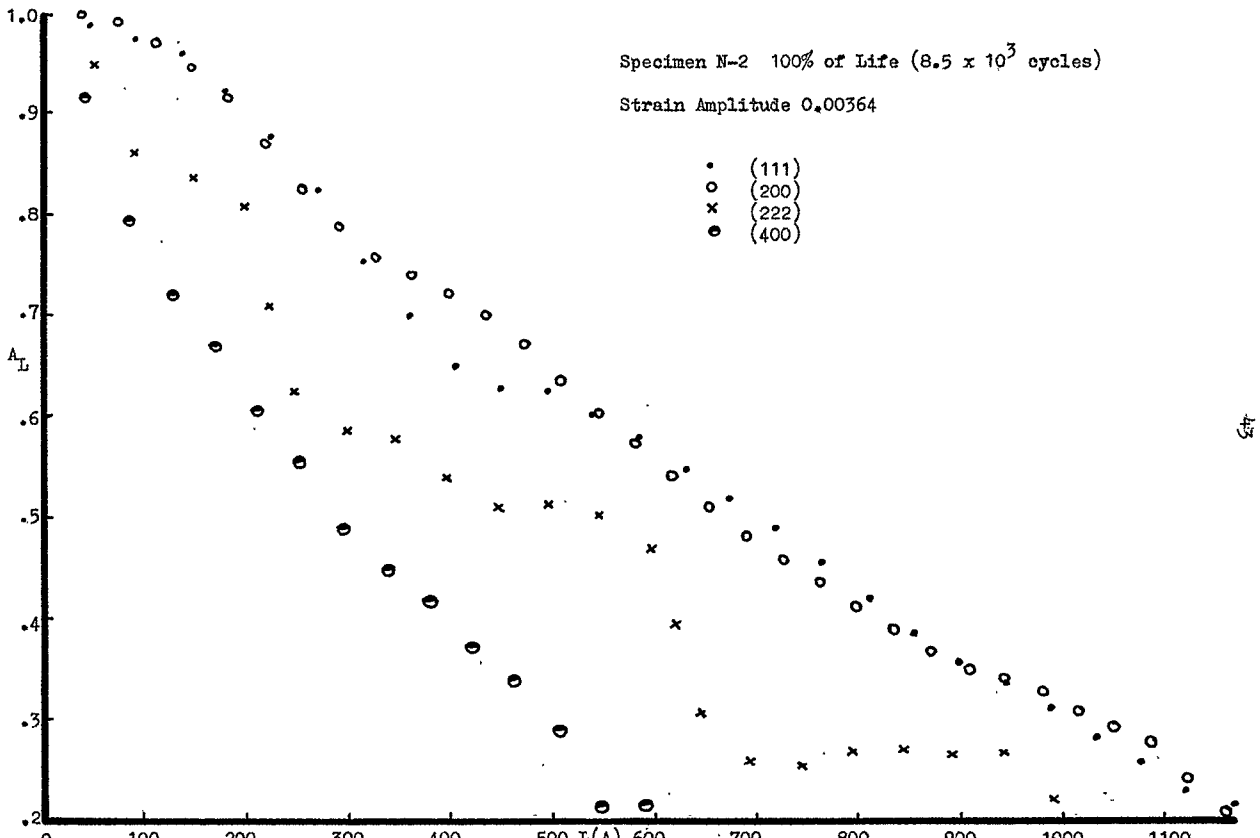
Specimen N-2 100% of Life (8.5 x 10^3 cycles)
Strain Amplitude 0.00364
(111)
(200)
(222)
(400)
A_L
1.0
.9
.8
.7
.6
.5
.4
.3
.2
0
100
200
300
400
500 L(A)
600
700
800
900
1000
1100

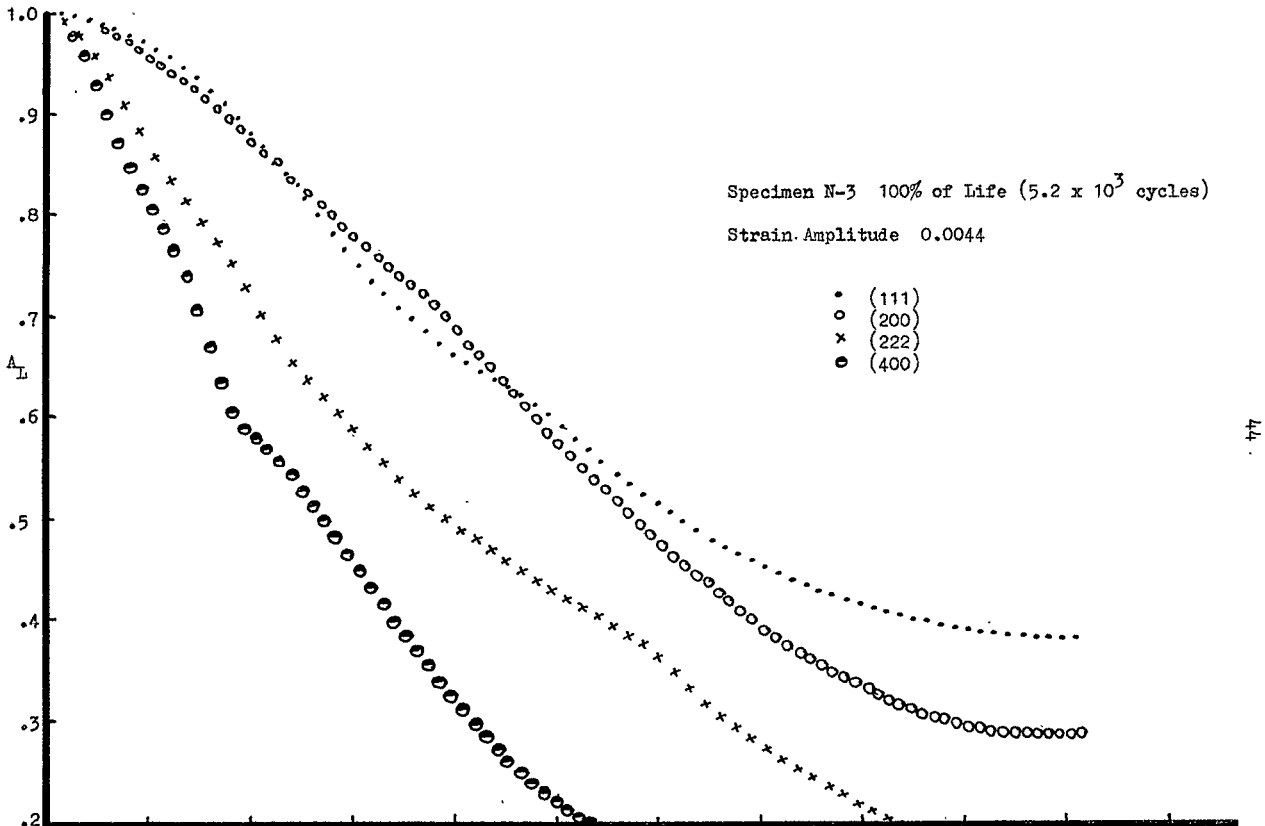
Specimen N-3 100% of Life (5.2 x 10^3 cycles)
Strain Amplitude 0.0044
(111)
(200)
(222)
(400)
A_L
L(A)
1.0
.9
.8
.7
.6
.5
.4
.3
.2
0
100
200
300
400
500
600
700
800
900
1000
1100

2. Change No.	3. Date Issued
17-538	12 MAY 67

1. Document affected-No. and title: SEE REMARKS

N66-28080

4. Authority for change: ☐ Input ☐ DDC ☐ AEC ☐ NASA ☐ Oral ☐ Written ☐ Other:

5. Name: ASHLEY

6. Issued by: SUTTON/CLAY

7. Changes
- a. Cancel, duplicate of:
- b. Cancel, superseded by:
- c. Withdraw from public sale
  - (1) Destroy doc & related papers
  - (2) Return doc & related papers to:
    - ☐ DDC-T ☐
- d. Change dist/avail code to:
- e. Other:

NOT REPRODUCIBLE, NOT AVAILABEL.

8. Remarks
N66-27026 (NASA TM X-56746)
N66-27067 (NASA TM X-56898)
N66-27196 (NASA TT F-8019)
N66-27242 (NASA CR-73379)
N66-27936 (NASA CR-75617)
N66-28080 (NASA CR-75754)
N66-28427 (NASA CR-75698)

Clearinghouse for Federal Scientific and Technical Information

U.S. DEPARTMENT OF COMMERCE
NATIONAL BUREAU OF STANDARDS

FORM AD-67(Rev.) JAN 67

☐ INPUT ☐ ANNOUNCEMENT ☐ CATALOG ☐ DDC

1 STOCK LOCATION

2 DATE RECEIVED: YR 71 MO 08 DAY 27

3 RECEIPT TYPE & FORMAT: ☐ MAGNETIC TAPE; ☐ LOAN ☒ PC ☐ 35 MM ☐ CARDS; ☒ RETAIN ☐ MF ☐ 16 MM ☐ OTHER →

4 STOCK RECEIVED FOR SALE: PC 0 MF

5 LOAN DOCUMENT RETURNED: DUE OUT

6 TRANSACTION: NEW ITEM ☒ DUPE ☐ SUPERSEDES ☐ PRIOR NUMBER ☐

7

8 REPORT NUMBERS (XREF) ☐→: NASA-CR-75764

9 RELATED DOCUMENT ☐→

10 CONTRACTING OFFICE — BILLING CODE: NASA

11 NOT FULLY LEGIBLE ☒ COLOR ☐

12 SCREEN: ☐ REJECT; ☐ OBTAIN BETTER COPY ☐ OUT OF PRINT SOD; ☐ OBTAIN AUTHORITY ☐ ERRATA

13A ANNOUNCEMENT: VOL 68 ISSUE 26; ☐ USG ☐ TAB ☒ UNANN

13B FAS: ☐ YES ☒ NO

14 REPRODUCTION INSTRUCTIONS: BLOWBACK →

PRINT ↓	NO	1UP	2UP
NO	1	4	7
1UP	2	5	8
2UP	3	6	9
MIX	SAME SIZE	ORDER STOCK FROM	0

MAKE MICROFICHE: ☐ YES ☒ NO

15 PRESTOCK

	NO!	# COPIES
PC		
MF		0

PC DUE IN

SOURCE TO ORDER COPIES

16 REMARKS

17 ACCESSION NUMBER: N66-28080

18 PAGES: 49

19 SHEETS: —

20 LOW LIMIT: PC MF

21 ☐ SUBSCRIPTION

22 PRICES: ☒ U UNIT ☐ P PC →; ☐ E PC + MN BOX 16 ☐ M MN →

23A CATEGORY

24 DISTR CODE: —

25 INITIALS: ACC EQ A B

23B CATEGORY

26 FILL FROM: PAPER COPY ETC BX ☐↓ MICRONEGATIVE XM

27 PUBLIC RELEASABILITY: T

28 FORM & PRICE

1 ARCHIVES

FORM NTIS-77 (10/70)

DOCUMENT TRAVELER

NATIONAL TECHNICAL INFORMATION SERVICE
U. S. DEPARTMENT OF COMMERCE

DOCUMENT REQUEST

NASA SCIENTIFIC AND TECHNICAL INFORMATION FACILITY
Operated By TECHNICAL INFORMATION SERVICES COMPANY
POST OFFICE BOX 33 COLLEGE PARK MARYLAND 20740 TELEPHONE (301) 779 2121

DOCUMENT REQUESTED

A NASA ACCESSION NUMBER	B NACA/NASA REPORT NUMBER
1 N66-28080	OR

C. (PLEASE DO NOT WRITE IN THIS SPACE) TMF

D COPY TYPE REQUESTED: 16 ☒ CASE FILE ☒ MICROFICHE ☐ FULL SIZE

REQUESTER IDENTIFICATION

E REQUESTER'S FACILITY IDENT. NO	F REQUESTER'S CONTRACT NO
2523	

G AUTHORIZED SIGNATURE AND DATE.
MRS. PEGGY SHEA Aug 12 1970

TN

NOTE: For prompt service, please follow instructions on back of last copy

FF 492 DEC. 68 1 SHIPPING COPY

OTHER BIBLIOGRAPHIC INFORMATION (ESSENTIAL IF ITEMS "A" AND "B" ARE UNKNOWN)

H DOCUMENT TITLE	
I DATE OF REPORT	J AUTHOR(S).
K CORPORATE SOURCE	L CORPORATE REPORT NO.
	M CONTRACT NO

N. MAILING LABEL (must be imprinted on all copies, include zip code)

NATIONAL TECHNICAL INFORMATION SERVICE
SPRINGFIELD, VA. 22151
ATTN: INPUT

RESPONSE TO DOCUMENT REQUEST

(See item checked below for the specific reply to your request)

THE DOCUMENT YOU REQUESTED,

MAY BE OBTAINED FROM:

- ☐ (1) Superintendent of Documents, U S.G P.O., Washington, D C. 20401.
- ☐ (2) Clearinghouse for Federal Scientific & Technical Information Springfield Vi 22151
- ☐ (3) Defense Documentation Center, Cameron Station Alexandria, Va. 22314
- ☐ (4) _____

IS OUT OF STOCK AND NOT REPRODUCIBLE BECAUSE.

- ☒ (5) Copyrighted.
- ☐ (6) Journal Article
- ☐ (7) Purchase Item; contact source.
- ☐ (8) Not suitable for reproduction
- ☐ (9) Source prohibits reproduction.

HAS DISTRIBUTION LIMITATIONS WHICH PREVENT US FROM SATISFYING YOUF REQUEST.

Available from the Facility to

- ☐ (10) NASA only
- ☐ (11) NASA and its contractors only
- ☐ (12) U S Government Agencies onl
- ☐ (13) U S. Government Agencies anc Contractors only
- ☐ (14) Classified, our records do not indicate adequate clearance; contact your cognizant contracting agency
- ☐ (15) Classified document in Category _____; our records do not indicate that your organization has been certified access to that category
- ☐ (16) Non-NASA document and therefore available from the Facility only to NASA and its contractors; our records do not indicate that you are registered with us as a NASA contractor
- ☐ (17) Source controls and monitors all distribution.

IS NOT AVAILABLE FOR THE FOLLOWING ADMINISTRATIVE REASON:

- ☐ (18) Not available outside U S
- ☐ (19) Requires approval of another Government agency for release (Serv. Rept), this approval is being sought, you will be notified
- ☐ (20) Approval sought in #19 has been denied.
- ☐ (21) Contains proprietary information, requiring approval of responsible NASA Office for release (Spec Rel); this approval is being sought, you will be notified.
- ☐ (22) Approval sought in #21 has been denied.
- ☐ (23) Obsolete, withdrawn from circulation
- ☐ (24) Out of subject scope; not retained in Facility's collection.
- ☐ (25) Out of print, not to be reprinted or reproduced
- ☐ (26) Repeated attempts to obtain have been unsuccessful.

IS NOT YET AVAILABLE

Request again when announced in *STAR* or *CSTAR* journals

- ☐ (27) Availability is under review
- ☐ (28) Review Copy or Advance Copy stage of publication
- ☐ (29) Not yet published
- ☐ (30) Out of stock; being reprinted; will be forwarded
- ☐ (31) Not in Facility's collection; action has been taken to obtain copies, you will be notified

IS INADEQUATELY IDENTIFIED

- ☐ (32) Please furnish correct NACA/NASA accession number or report number or additional bibliographic information
- ☐ (33) Accession number or report number cited is not valid check reference

IS NOT AVAILABLE IN COPY TYPE REQUESTED:

- ☐ (34) Available in microfiche only a microfiche is enclosed
- ☐ (35) Available in printed copy only

IS NOT AVAILABLE IN MULTIPLE COPIES:

- ☐ (36) Enclosed is one photocopy and one microfiche; the microfiche may be utilized as a reproducible master